ELSEVIER

A multiscale thermomechanical model for cubic to tetragonal martensitic phase transformations

S. Turteltaub *, A.S.J. Suiker

Faculty of Aerospace Engineering, Delft University of Technology, Kluyverweg 1, 2629 HS Delft, The Netherlands

Abstract

We develop a multiscale thermomechanical model to analyze martensitic phase transformations from a cubic crystalline lattice to a tetragonal crystalline lattice. The model is intended for simulating the thermomechanical response of single-crystal grains of austenite. Based on the geometrically nonlinear theory of martensitic transformations, we incorporate microstructural effects from several subgrain length scales. The effective stiffness tensor at the grain level is obtained through an averaging scheme, and preserves crystallographic information from the lattice scale as well as the influence of volumetric changes due to the transformation. The model further incorporates a transformation criterion that includes a surface energy term, which takes into account the creation of interfaces between martensite and austenite. These effects, which are often neglected in martensitic transformation models, thus appear explicitly in the expression of the transformation driving force that controls the onset and evolution of the transformation. In the derivation of the transformation driving force, we clarify the relations between different combinations of thermodynamic potentials and state variables. The predictions of the model are illustrated by analyzing the response of a phase-changing material subjected to various types of deformations. Although the model is developed for cubic to tetragonal transformations, it can be adapted to simulate martensitic transformations for other crystalline structures.
© 2005 Elsevier Ltd. All rights reserved.

Keywords: Phase transformation; Multiscale; Martensite; Austenite; Driving force

1. Introduction

Driven by the technological necessity to create efficient structural designs, there is a constant need to develop materials with enhanced structural and functional properties. Among the physical phenomena that

---

* Corresponding author. Tel.: +31152785360; fax: +31152611465.
 E-mail addresses: s.r.turteltaub@lr.tudelft.nl (S. Turteltaub), a.suiker@lr.tudelft.nl (A.S.J. Suiker).

can be exploited to improve the performance of materials, solid-state martensitic transformations in steels and metal alloys occupy a prominent position. Martensitic transformations play a role in the thermal processing of these materials (e.g., dual phase steels and maraging steels) as well as during their forming and operation (e.g., austenitic alloys such as Fe–Ni–C and Fe–Mn–C and multiphase steels assisted by transformation-induced plasticity). The transformation of austenite into martensite in multiphase carbon steels is the underlying mechanism for improving their overall yield strength and ductility. Martensitic transformations are also relevant for functional materials, such as shape memory alloys, where the pseudoelasticity and shape memory effects are related to a reversible phase change. Although the current market for shape memory alloys is limited to a few specialized applications, their potential large-scale use remains nonetheless significant. A thorough understanding of martensitic transformations is therefore important, particularly in view of devising a systematic way to improve mechanical and functional characteristics of steels and metal alloys.

Various constitutive models for reversible and irreversible martensitic transformations have been proposed in the literature (see, e.g., Olson and Cohen, 1975; Leblond et al., 1986a,b; Stringfellow et al., 1992; Bhattacharyya and Weng, 1994; Marketz and Fischer, 1994, 1995; Diani and Parks, 1998; Huang and Brinson, 1999; Idesman et al., 1999; Levitas et al., 1999; Govindjee and Miehe, 2001; Thamburaja and Anand, 2001; Anand and Gurtin, 2003). Some of these models have a strongly phenomenological nature, whereas other models incorporate microstructural information through the use of averaging techniques. The present model falls within the latter category, where microstructural information is included by introducing a hierarchical series of length scales connected to relevant substructures that govern the stability of austenite. We take explicitly into account the orientation of the austenitic and martensitic crystal lattices with respect to the local stress field, as well as their anisotropic elastic properties. To this end, we use the theory of martensitic transformations originally proposed by Wechsler et al. (1953) and further refined by Ball and James (1987) (see also Bhattacharya, 1993; Hane and Shield, 1998, 1999; James and Hane, 2000). We employ this information within an averaging scheme in order to estimate the effective elasticity tensor at the grain level. The effective stiffness tensor thus preserves crystallographic characteristics from lower length scales as well as the influence of volumetric changes due to the transformation. For estimating the effective mechanical properties, the present model assumes that the austenitic phase is cubic and the martensitic phase is tetragonal. Nonetheless, most of the analysis carries over for other types of crystalline structures.

The transformation criterion in the model is based on a thermodynamically-consistent approach similar to the one employed by Fischer et al. (1998) for TRIP-assisted steels and by Anand and Gurtin (2003) and Jannetti et al. (2004) for shape memory alloys. Through the incorporation of the small scale kinematic characteristics by means of an averaging scheme, we circumvent the need of additional balance principles, as proposed by Anand and Gurtin (2003). Moreover, the present model incorporates the effect of the energy stored in austenite-martensite interfaces and its corresponding contribution to the transformation driving force. In the derivation of the transformation driving force, we study the relations between the internal, Helmholtz and Gibbs energies in terms of state variables that characterize the transformation process.

As a general scheme of notation, scalars are written as lightface italic letters (e.g., a, b), vectors as boldface lowercase letters (e.g., $\boldsymbol{a}$, $\boldsymbol{b}$), second-order tensors as boldface uppercase letters (e.g., $\boldsymbol{A}$, $\boldsymbol{B}$) and fourth-order tensors as blackboard bold capital letters (e.g., $\mathbb{A}$, $\mathbb{B}$). For vectors and tensors, Cartesian components are denoted as a_i, A_{ij} and A_{ijkl}. The action of a second-order tensor on a vector is denoted as $\boldsymbol{Ba}$ (in components $B_{ij}a_j$, with implicit summation on repeated indices) and the action of a fourth-order tensor on a second-order tensor is denoted as $\mathbb{B}\boldsymbol{A}$ (i.e., $B_{ijkl}A_{kl}$). Composition of two second-order tensors is denoted as $\boldsymbol{AB}$ (i.e., $A_{ij}B_{jk}$). The tensor product between two vectors is denoted as $\boldsymbol{a} \otimes \boldsymbol{b}$ (i.e., a_ib_j). All inner products are denoted with a single dot between the quantities, i.e., $\boldsymbol{a} \cdot \boldsymbol{b}$ for vectors and $\boldsymbol{A} \cdot \boldsymbol{B}$ for tensors (in components, a_ib_i and $A_{ij}B_{ij}$ respectively). A material time derivative is denoted by a superimposed dot. Additional notation is introduced where required.

The paper is organized as follows: The various length scales as well as the kinematic analysis are developed in Section 2. Based on taking successive averages across length scales, we derive an expression for the mesoscale effective stiffness tensor in Section 3. In Section 4 we explore the restrictions imposed by the second law of thermodynamics in order to identify the transformation driving force. We construct a particular form of the Helmholtz energy and derive an expression for the driving force in Section 5. In addition, we specify the transformation kinetics and summarize the main equations of the model. The response of a phase-changing material under basic loading conditions is illustrated in Section 6. Some closing remarks are provided in Section 7.

2. Kinematics for martensitic transformations

The martensitic transformation model presented here is intended for a single crystal of austenite, which can be found in a fully-austenitic alloy or in an isolated austenitic grain in a multiphase steel, see Figs. 1a and b, respectively. Upon application of mechanical and/or thermal loadings, the austenite can transform into martensite. Martensitic transformations are classified as displacive, i.e., they are characterized by a diffusionless, coordinated rearrangement of the crystalline lattices. To analyze this transformation, we first describe the kinematics. This description is done at different length scales that are connected to each other through sequential averaging procedures.

2.1. Scales of observation and kinematic assumptions

In the present model we focus attention on thin-plate twinned martensite as a product phase. Thin-plate martensite has straight interfaces with the adjacent austenite and has a very uniform twinned substructure, where the twins extend across the plate thickness. This type of martensite is commonly observed in shape memory alloys (James and Hane, 2000) as well as in multiphase carbon steels with a local carbon concentration above 1.4 wt.% and a martensitic transformation temperature (M_s) below room temperature (Rao and Rashid, 1997; Sugimoto et al., 1997).

The substructures in thin-plate martensite are shown schematically in Fig. 2. Fig. 2a, which corresponds to the internal structure shown in Fig. 1, is often on the order of a few microns. In addition, we distinguish three finer scales of interest. For future reference, the four scales are called the *mesoscale*, the *upper microscale*, the *lower microscale* and the *lattice scale*. As a result of mechanical loading, regions of martensite may appear inside the austenitic island shown in Fig. 2a (mesoscale). At a smaller scale of observation, these martensitic regions often emerge as plates with specific orientations, see Fig. 2b (upper microscale). Further magnification of a martensitic plate reveals a layered structure, as shown in Fig. 2c (lower microscale). This layered structure consists of tetragonal martensite,[1] which is shown at the lattice scale in Fig. 2d. We formally treat the deformation inside an isolated grain of austenite as thermoelastic. The model is thus intended for *stress-assisted* martensitic transformations, rather than for the so-called strain-induced martensitic transformations that are characterized by plastic deformations in the austenitic parent phase.

2.2. Transformation kinematics: from lattice to lower microscale

At the lattice scale, martensite is found as one out of three possible tetragonal *variants*.[2] The word "variant" is used here according to notions of group theory, see e.g., James and Hane (2000). The Bain

---

[1] In a cubic to tetragonal transformation.

[2] Since the point group of a cubic lattice of austenite is composed of 24 rotations and the point group of a tetragonal lattice of martensite contains 8 rotations, it follows that there are 24/8 = 3 distinct variants of tetragonal martensite.
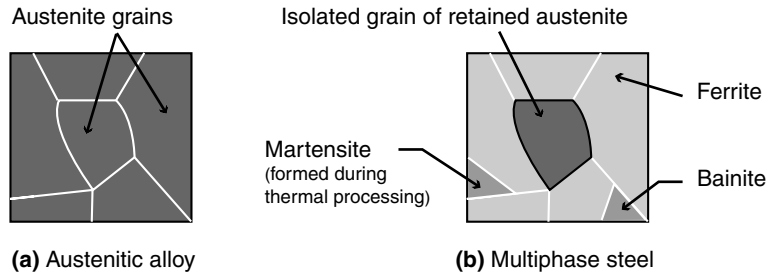
Fig. 1. Austenite grain: (a) polycrystalline austenitic alloy, (b) isolated grain inside a ferrite-based matrix in a multiphase ssteel.
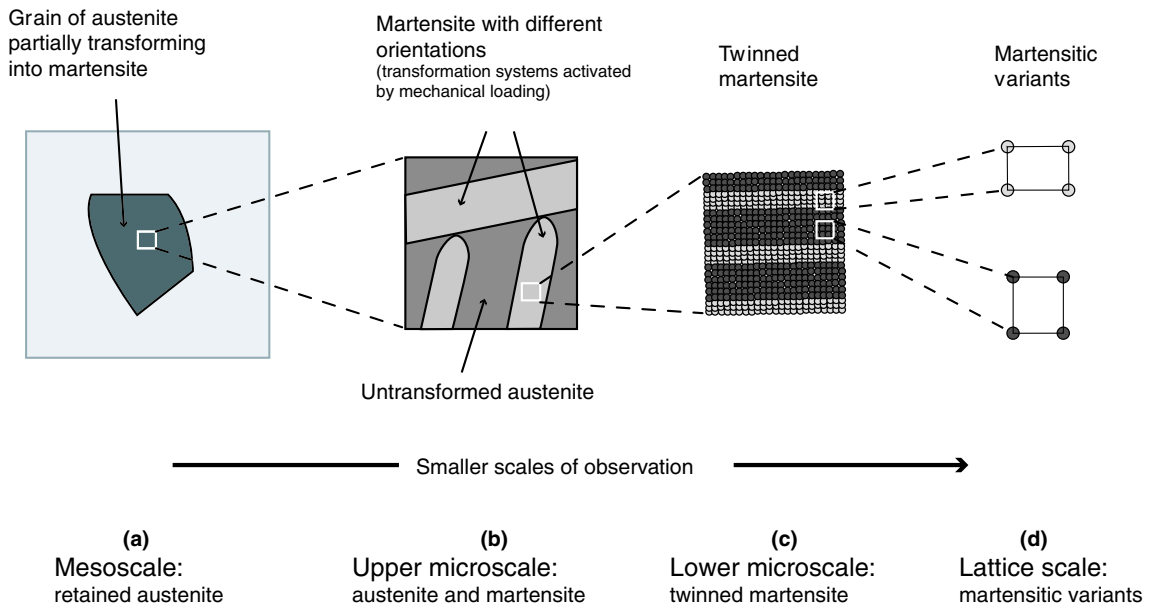

Fig. 2. Scales of observation.

correspondence model is illustrated in Fig. 3 for the case of a face-centered cubic (FCC) austenitic lattice and a body-centered tetragonal (BCT) martensitic lattice. The transformation is interpreted, according to Bain's model, as a stretch along a direction perpendicular to a face of the cubic unit cell and an equibiaxial stretch in a plane parallel to that face. The transformation from austenite into one variant of martensite is illustrated in the inset of Fig. 3. The cubic lattice parameter (austenite) is denoted as a^{A} and the tetragonal lattice parameters (martensite) are denoted as a^{M} and c^{M}. Adopting the Cauchy–Born hypothesis (see, e.g., Zanzotto, 1996) to relate the deformation of a discrete lattice to the kinematics of a continuum, the principal stretches α_{tr} and β_{tr} for the austenite to martensite transformation can be obtained as

$$\alpha_{\mathrm{tr}} = \sqrt{2}\frac{a^{\mathrm{M}}}{a^{\mathrm{A}}}, \beta_{\mathrm{tr}} = \frac{c^{\mathrm{M}}}{a^{\mathrm{A}}}, \tag{1}$$

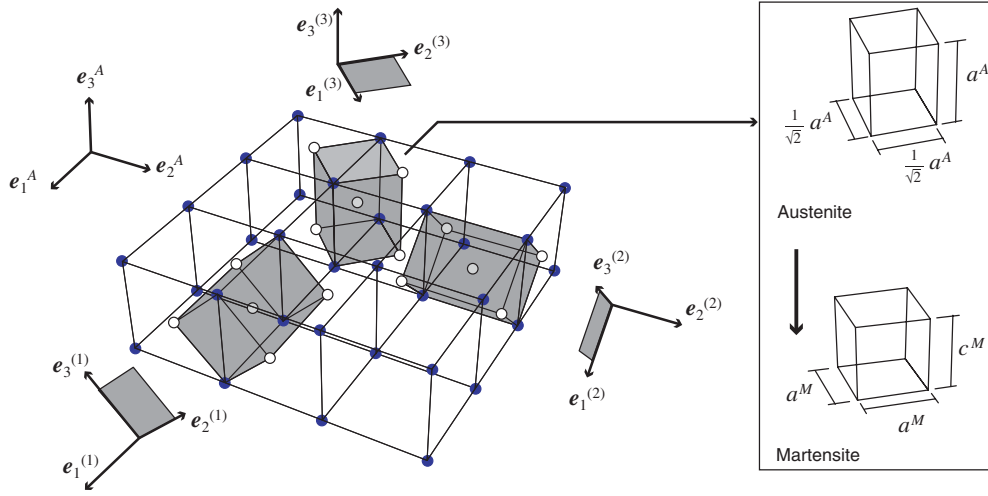as shown schematically in the inset of Fig. 3.

Fig. 3. Martensitic variants, lattice parameters and basis vectors. The three tetragonal variants are shown in the original cubic lattice of austenite. Black circles represent corner locations while white circles refer to face locations (only face locations in the tetragonal lattices are shown).

For the lattice of austenite, we use an orthonormal basis $\{e_i^A\}_{i=1}^3$ aligned with the cubic axes of the untransformed austenite. Introduce for each of the three variants a basis $\{e_i^{(\beta)}\}_{i=1}^3$ ($\beta = 1, 2, 3$) and define three rotation tensors $R_*^{(\beta)}$ such that

$$e_i^{(\beta)} = R_*^{(\beta)} e_i^A. \tag{2}$$

The components of the rotations $R_*^{(\beta)}$, in the austenite tensor basis $\{e_i^A \otimes e_j^A\}_{i,j=1}^3$, are given by

$$[R_*^{(1)}]_A := \begin{pmatrix} 1 & 0 & 0 \\ 0 & \frac{\sqrt{2}}{2} & -\frac{\sqrt{2}}{2} \\ 0 & \frac{\sqrt{2}}{2} & \frac{\sqrt{2}}{2} \end{pmatrix}_A, \quad [R_*^{(2)}]_A := \begin{pmatrix} \frac{\sqrt{2}}{2} & 0 & \frac{\sqrt{2}}{2} \\ 0 & 1 & 0 \\ -\frac{\sqrt{2}}{2} & 0 & \frac{\sqrt{2}}{2} \end{pmatrix}_A, \quad [R_*^{(3)}]_A := \begin{pmatrix} \frac{\sqrt{2}}{2} & -\frac{\sqrt{2}}{2} & 0 \\ \frac{\sqrt{2}}{2} & \frac{\sqrt{2}}{2} & 0 \\ 0 & 0 & 1 \end{pmatrix}_A. \tag{3}$$

The stretch tensors $U^{(\beta)}$ that characterize the transformation from austenite to variant $\beta = 1, 2, 3$ of martensite are

$$U^{(\beta)} = \alpha_{tr} I + (\beta_{tr} - \alpha_{tr}) e_\beta^{(\beta)} \otimes e_\beta^{(\beta)} \tag{4}$$

with I the identity tensor. As can be seen from the spectral decomposition of the stretch tensor given by (4), the basis vectors $\{e_i^{(\beta)}\}_{i=1}^3$ also correspond to the eigenvectors of $U^{(\beta)}$. The ordering of the eigenvectors is chosen such that $e_\beta^{(\beta)}$ corresponds to the eigenvalue β_{tr}. The two other eigenvectors can be chosen arbitrarily in the plane perpendicular to $e_\beta^{(\beta)}$. A specific choice is given by Eqs. (2) and (3). It can be observed from Fig. 3 that $e_\beta^{(\beta)} = e_\beta^A$. Combining this relation with (4) leads to the following expression for the transformation stretch tensor of variant β:

$$U^{(\beta)} = \alpha_{tr} I + (\beta_{tr} - \alpha_{tr}) e_\beta^A \otimes e_\beta^A. \tag{5}$$

Although at the lattice scale martensite appears as one of the three variants shown in Fig. 3, at larger length scales, the basic variants are often arranged in specific twinned structures, which are discussed in the next subsection.

2.3. Transformation kinematics: from lower to upper microscale

Coherent interfaces between martensite and austenite are often achieved via specific pairwise arrangements of twin-related variants of martensite (i.e., twinned martensite). Each such special arrangement of twinned martensite will be referred to as a *transformation system*. In cubic to tetragonal transformations there are 24 distinct transformation systems (Hane and Shield, 1998) that will be henceforth enumerated with the index $\alpha = 1, \ldots, N$, where $N = 24$. Each transformation system consists of two variants of martensite in specific proportions and orientations. An example of a transformation system is shown in Fig. 4, which has been constructed using the theory of martensitic transformations (Wechsler et al., 1953; Ball and James, 1987). It is important to point out that, in this theory, all phases (sufficiently away from interfaces) are assumed to be stress free. As a working assumption, we will consider that the main characteristics of the twins persist under the presence of an applied stress (e.g., we neglect effects such as detwinning during loading).

Consider a transformation system α where on one side of the interface there is austenite and on the other side there is twinned martensite composed of variants β_1 and β_2, layered in volumetric proportions $\lambda^{(\alpha,\beta_1)}$ and $\lambda^{(\alpha,\beta_2)}$, with $\lambda^{(\alpha,\beta_1)} + \lambda^{(\alpha,\beta_2)} = 1$. If one assumes a *stress-free* state, the deformation gradient for austenite is $\boldsymbol{F}_{\mathrm{tr}}^{\mathrm{A}} = \boldsymbol{I}$ and the deformation gradients for the two martensitic variants are

$$\boldsymbol{F}_{\mathrm{tr}}^{(\alpha,\beta_1)} = \boldsymbol{Q}^{(\alpha,\beta_1)} \boldsymbol{U}^{(\beta_1)}, \quad \boldsymbol{F}_{\mathrm{tr}}^{(\alpha,\beta_2)} = \boldsymbol{Q}^{(\alpha,\beta_2)} \boldsymbol{U}^{(\beta_2)}, \tag{6}$$

where $\boldsymbol{U}^{(\beta_1)}$ and $\boldsymbol{U}^{(\beta_2)}$ are the transformation stretch tensors introduced in (4) and $\boldsymbol{Q}^{(\alpha,\beta_1)}$ and $\boldsymbol{Q}^{(\alpha,\beta_2)}$ are rotations of the variants with respect to the lattice of austenite. The average deformation gradient $\boldsymbol{F}_{\mathrm{tr}}^{(\alpha)}$ of the transformation system α is given by

$$\boldsymbol{F}_{\mathrm{tr}}^{(\alpha)} = \lambda^{(\alpha,\beta_1)} \boldsymbol{F}_{\mathrm{tr}}^{(\alpha,\beta_1)} + \lambda^{(\alpha,\beta_2)} \boldsymbol{F}_{\mathrm{tr}}^{(\alpha,\beta_2)}. \tag{7}$$

A condition that needs to be satisfied by a coherent interface is that the difference between the deformation gradients on each side of the interface has to be a rank-one tensor. This is the Hadamard jump condition
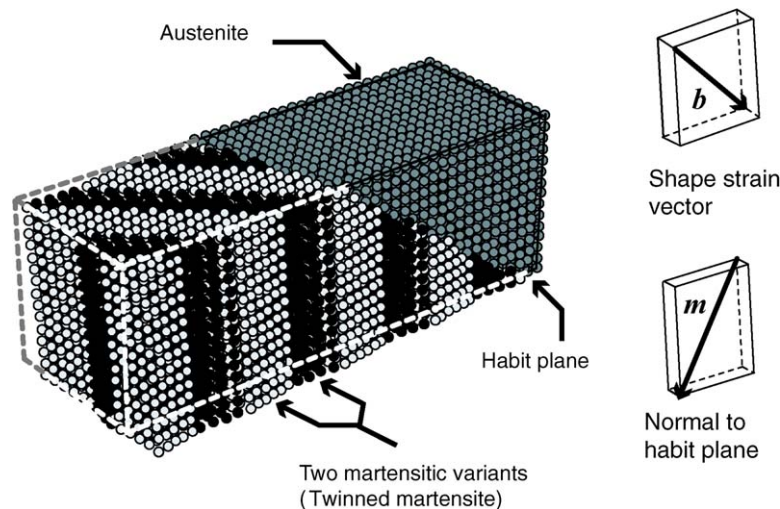

Fig. 4. Twinned martensite and austenite. The small spheres correspond to the corner locations of the cubic and tetragonal lattices. The vector $\boldsymbol{m}$ is normal to the habit plane and the vector $\boldsymbol{b}$ represents the average shape strain. The locations of the lattice corners were computed following the theory of Ball and James (1987).

for deformation gradients which, for an austenite/twinned martensite interface, leads to the *habit plane equation* expressed as (James and Hane, 2000)

$$F_{\mathrm{tr}}^{(\alpha)} - F_{\mathrm{tr}}^{\mathrm{A}} = \bar{R}^{(\alpha)}\left(\lambda^{(\alpha,\beta_1)} R^{(\alpha)} U^{(\beta_1)} + \lambda^{(\alpha,\beta_2)} U^{(\beta_2)}\right) - I = b^{(\alpha)} \otimes m^{(\alpha)}. \tag{8}$$

In (8), $m^{(\alpha)}$ is the unit vector normal to the habit plane (interface between austenite and twinned martensite), $b^{(\alpha)}$ is the (average) *shape strain vector* and the rotations $R^{(\alpha)}$ and $\bar{R}^{(\alpha)}$ are defined as

$$R^{(\alpha)} := (Q^{(\alpha,\beta_2)})^{\mathrm{T}} Q^{(\alpha,\beta_1)}, \quad \bar{R}^{(\alpha)} := Q^{(\alpha,\beta_2)}. \tag{9}$$

As can be noted from (8), the stress-free twinned martensite in the transformation system α has an average deformation gradient equal to

$$F_{\mathrm{tr}}^{(\alpha)} = I + \gamma^{(\alpha)}, \tag{10}$$

where

$$\gamma^{(\alpha)} := \gamma_{\mathrm{T}} \hat{b}^{(\alpha)} \otimes m^{(\alpha)}. \tag{11}$$

In (11) the shape strain magnitude is $\gamma_{\mathrm{T}} := \| b^{(\alpha)} \|$ and the normalized shape strain vector is $\hat{b}^{(\alpha)} := b^{(\alpha)}/\gamma_{\mathrm{T}}$. One can show that for all transformation systems α the shape strain magnitude is the same.

The procedure to compute the deformation gradient $F_{\mathrm{tr}}^{(\alpha)}$ is as follows: the principal stretches α_{tr} and β_{tr} are calculated from (1) and the transformation stretch tensors in the lattice basis of austenite are obtained from (5). Subsequently, this information is used as input to the algorithm outlined by Hane and Shield (1998, 1999) to compute the vectors $b^{(\alpha)}$ and $m^{(\alpha)}$ for all $\alpha = 1, \ldots, 24$. Additionally, the same algorithm provides the twin volume fractions $\lambda^{(\alpha,\beta_1)}$ and $\lambda^{(\alpha,\beta_2)}$ and the rotation tensors $R^{(\alpha)}$ and $\bar{R}^{(\alpha)}$; these parameters will be used in Section 3 for estimating the effective elastic properties of the twinned martensite. Observe that, since the rotations $R^{(\alpha)}$ and $\bar{R}^{(\alpha)}$ are computed, there is no need to assume a priori an orientation relationship such as Kurdjumov-Sachs or Nishiyama-Wassermann (Christian, 2002).

Up to this point we have only considered the transformation kinematics. In the next section we consider the total deformation by introducing an elastic contribution. Following the viewpoint of Jannetti et al. (2004), the mesoscale deformation gradient is related to a volume average of the deformation gradients associated with each phase in a representative volume element.

2.4. Elastic and transformation kinematics: from upper microscale to mesoscale

In order to connect the kinematic descriptions from the upper microscale to the mesoscale, let us consider a representative volume element (RVE) at the upper microscale level, shown in Fig. 2b. In this setting, we construct a *reference* configuration from the region occupied by the undistorted austenite with a given crystal lattice orientation. The reference configuration for the upper microscale kinematics is inherited from the mesoscale, as depicted in Fig. 5. Further, let x be the location of a *mesoscale material point* in the reference configuration and let Y_x be the corresponding RVE centered at x. By adopting two kinematic assumptions, we will show below that the mesoscale deformation gradient $F = F(x, t)$ at point x and time t can be decomposed as

$$F = F_{\mathrm{e}} F_{\mathrm{tr}}, \tag{12}$$

where F_{e} and F_{tr} represent the elastic and the transformation parts of the deformation gradient, respectively. This decomposition is equivalent to that used in large deformation plasticity, i.e., $F = F_{\mathrm{e}} F_{\mathrm{p}}$ (Lee, 1969; Hill and Rice, 1972; Havner, 1973), where the transformation deformation gradient F_{tr} plays a similar role as the plastic deformation gradient F_{p}. In connection with the decomposition (12), we introduce an *intermediate configuration* (unstressed) and a *current configuration* as shown in Fig. 5. The vectors $y = F_{\mathrm{tr}} x$
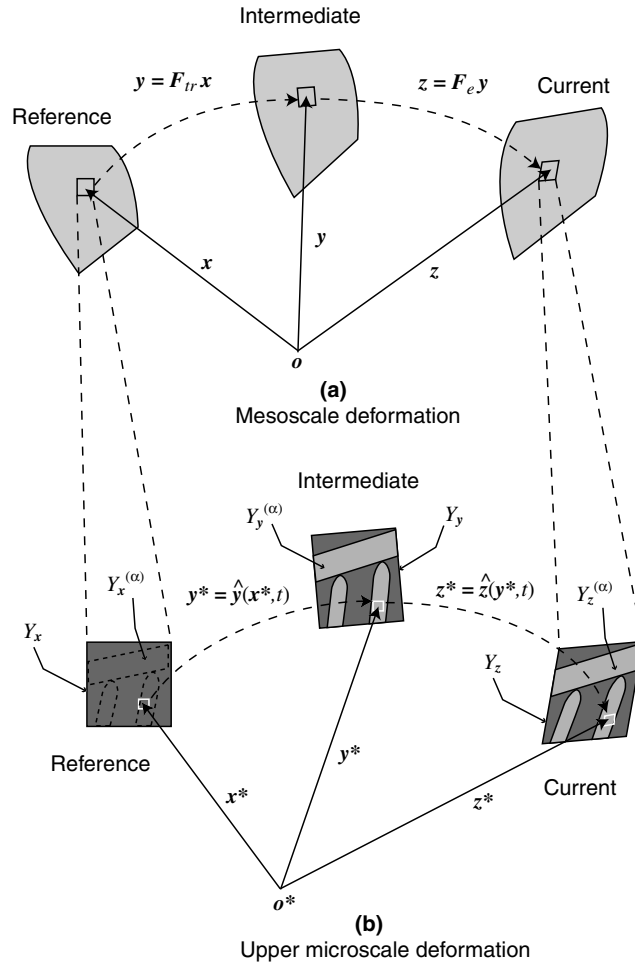
Fig. 5. Reference, intermediate and current configurations at the (a) mesoscale level and (b) upper microscale level.

and $z = F_e y$ correspond to the location of the center of Y_x in the intermediate and the current configurations,[3] respectively, where $F_{tr} = F_{tr}(x, t)$ and $F_e = F_e(y, t)$.

At the upper microscale level, we denote by x^* the location of a microscale material point inside Y_x. As shown in Fig. 5, the deformation due to the martensitic transformation is characterized by a function $\hat{y}$ whereas the elastic deformation is characterized by a function $\hat{z}$. To make a connection with the mesoscale kinematics, we consider deformations such that the boundary of Y_x is mapped in accordance with

$$y^* = F_{tr} x^*, \quad z^* = F_e y^* \quad \forall x^* \in \partial Y_x, \tag{13}$$

where as before, $F_{tr} = F_{tr}(x, t)$ and $F_e = F_e(y, t)$.

We note that the inelastic deformation at the microscale $\hat{y}$ should be accompanied by a small elastic contribution in order to maintain coherent interfaces between austenite and twinned martensite as well as

---

[3] Strictly speaking the vectors y and z are given by $y = F_{tr} x + c$ and $z = F_e y + d$ but for simplicity and without loss of generality we have assumed that the rigid body translations c and d are zero.

coherent interfaces between different twins (Ball and James, 1987). Nonetheless, we assume that most of the elastic deformation is characterized by $\hat{z}$. We will a posteriori take into account the effect of local elastic deformations at the interfaces by means of a surface energy contribution (see Section 5).

We now consider *subregions* inside Y_x where martensite nucleates. We denote as $Y_x^{(\alpha)}(t)$ the subregion occupied by the transformation system α at time t. Observe that these subregions are defined in the reference configuration even though the martensite is physically present in the current configuration. We reserve $\alpha = 0$ for the subregion occupied by untransformed austenite and denote the volume of Y_x as $|Y_x|$. In view of (12 and 13), and applying the divergence theorem, it follows that

$$F(x, t) = \frac{1}{|Y_x|} \int_{Y_x} \nabla_{x^*} \hat{z}(\hat{y}(x^*, t), t) \, dv_{x^*}.$$

Since $Y_x = \bigcup_{\alpha=0}^{N} Y_x^{(\alpha)}(t)$ and using the chain rule, the above relation can be expressed as

$$F(x, t) = \frac{1}{|Y_x|} \sum_{\alpha=0}^{N} \int_{Y_x^{(\alpha)}(t)} \nabla_{y^*} \hat{z}(y^*, t) \nabla_{x^*} \hat{y}(x^*, t) \, dv_{x^*}, \tag{14}$$

where $y^* = \hat{y}(x^*, t)$ and N is the total number of transformation systems as defined in Section 2.3. We now assume that the transformation deformation gradient is *constant* in each subregion $Y_x^{(\alpha)}(t)$ and equal to the transformation deformation gradient of the corresponding transformation system α, i.e.,

$$\nabla_{x^*} \hat{y}(x^*, t) = F_{tr}^{(\alpha)} \quad \forall x^* \in Y_x^{(\alpha)}(t), \quad \alpha = 0, \dots, N, \tag{15}$$

where $F_{tr}^{(\alpha)}$ is given by (10). Eq. (14), under assumption (15), becomes

$$F(x, t) = \frac{1}{|Y_x|} \sum_{\alpha=0}^{N} \left(\frac{1}{J_{tr}^{(\alpha)}} \int_{Y_y^{(\alpha)}(t)} \nabla_{y^*} \hat{z}(y^*, t) \, dv_{y^*} \right) F_{tr}^{(\alpha)}, \tag{16}$$

where $Y_y^{(\alpha)}(t)$ is the region occupied by $Y_x^{(\alpha)}(t)$ in the intermediate configuration and

$$J_{tr}^{(\alpha)} := \det F_{tr}^{(\alpha)} \tag{17}$$

for each α. Eq. (16) can be expressed as

$$F = \sum_{\alpha=0}^{N} \xi^{(\alpha)} F_e^{(\alpha)} F_{tr}^{(\alpha)}, \tag{18}$$

where

$$F_e^{(\alpha)} := \frac{1}{|Y_y^{(\alpha)}(t)|} \int_{Y_y^{(\alpha)}(t)} \nabla_{y^*} \hat{z}(y^*, t) \, dv_{y^*} \tag{19}$$

is the average elastic deformation gradient in each subregion $Y_y^{(\alpha)}(t)$ and

$$\xi^{(\alpha)} = \xi^{(\alpha)}(x, t) := \frac{1}{|Y_x|} \frac{|Y_y^{(\alpha)}(t)|}{J_{tr}^{(\alpha)}} = \frac{|Y_x^{(\alpha)}(t)|}{|Y_x|}. \tag{20}$$

The parameter $\xi^{(\alpha)}$ corresponds to the mesoscale volume fraction of the subregions $Y_x^{(\alpha)}(t)$ occupied by the transformation system α (with $\alpha = 0$ representing austenite). Observe that these volume fractions are measured in the reference configuration. Since we assume that austenite can only transform into one or more transformation systems α (with $1 \leqslant \alpha \leqslant 24$), the volume fractions must satisfy the following condition:

$$\xi^{(0)} = 1 - \sum_{\alpha=1}^{N} \xi^{(\alpha)}. \tag{21}$$

In addition to the kinematic assumption (15), we introduce a second kinematic assumption, namely that all *average* elastic deformation gradients $\boldsymbol{F}_e^{(\alpha)}$ are equal to a common value $\boldsymbol{F}_e$, i.e.,

$$\boldsymbol{F}_e^{(\alpha)} = \boldsymbol{F}_e, \quad \alpha = 0, \ldots, N. \tag{22}$$

Enforcing this assumption, the decomposition (12) follows from (18) with the transformation deformation gradient given by

$$\boldsymbol{F}_{tr} = \sum_{\alpha=0}^{N} \xi^{(\alpha)} \boldsymbol{F}_{tr}^{(\alpha)}. \tag{23}$$

In view of (10), (21) and (23), with $\gamma^{(0)} = 0$ for austenite, the transformation deformation gradient can be expressed as

$$\boldsymbol{F}_{tr} = \boldsymbol{I} + \sum_{\alpha=1}^{N} \xi^{(\alpha)} \boldsymbol{\gamma}^{(\alpha)}. \tag{24}$$

The present model has some formal similarities with crystal plasticity models where transformation systems play an equivalent role to slip systems. However, as opposed to crystal plasticity, $\boldsymbol{\gamma}^{(\alpha)}$ is the tensor product of two *nonorthogonal* vectors $\boldsymbol{b}^{(\alpha)}$ and $\boldsymbol{m}^{(\alpha)}$, where the nonorthogonality is related to the nonzero volumetric change caused by the transformation. We note that the material time derivative of $\boldsymbol{F}_{tr}$ is given by

$$\dot{\boldsymbol{F}}_{tr} = \sum_{\alpha=1}^{N} \dot{\xi}^{(\alpha)} \boldsymbol{\gamma}^{(\alpha)}. \tag{25}$$

The above kinematic description is different than the one adopted by Thamburaja and Anand (2001) and Anand and Gurtin (2003), which is based on an analogy with crystal plasticity. The rate of volume fraction $\dot{\xi}^{(\alpha)}$ in (25) will be obtained by means of a kinetic law, as further explained in Sections 4 and 5.

3. Stress and effective elastic stiffness in austenite and martensite

To determine the stress and the effective elastic stiffness at the mesoscopic level, we assume for all scales that the second Piola–Kirchhoff stress in the intermediate configuration is related linearly to the elastic Green–Lagrange strain tensor. The relation between the stress and elastic strain measures at each scale is given in terms of a corresponding effective elasticity tensor. We start from the lower microscale and exploit information about the twinned martensite to determine the effective stiffness at the upper microscale. Subsequently, we average the constitutive relations at the upper microscale to determine the stress and effective stiffness at the mesoscale.

3.1. Effective stiffness: from lower- to upper microscale

Consider an RVE at the *lower* microscale as shown in Fig. 2c. RVEs at that level might be composed of *either* austenite *or* one of the transformation systems α. Suppose first that the RVE corresponds to a region occupied by the transformation system α composed of variants β_1 and β_2 of martensite layered in proportions $\lambda^{(\alpha,\beta_1)}$ and $\lambda^{(\alpha,\beta_2)}$. Fig. 2c corresponds schematically to the case of an RVE occupied by one of the transformation systems.

Assuming that the elastic deformation in both martensitic variants β_1 and β_2 is the same,[4] then the effective elastic stiffness $\mathbb{C}^{(\alpha)}$ for the transformation system α is

$$\mathbb{C}^{(\alpha)} = \lambda^{(\alpha,\beta_1)}\mathbb{E}^{(\beta_1)} + \lambda^{(\alpha,\beta_2)}\mathbb{E}^{(\beta_2)}, \quad \alpha = 1, \ldots, N, \tag{26}$$

where $\mathbb{E}^{(\beta)}$ denotes the elasticity tensor of variant β at the lower microscale level. As mentioned in Section 2.3, the volume fractions $\lambda^{(\alpha,\beta_1)}$ and $\lambda^{(\alpha,\beta_2)}$ can be computed from the algorithm outlined in Hane and Shield (1998). We note that the volume fractions $\lambda^{(\alpha,\beta)}$ and the stiffnesses $\mathbb{E}^{(\beta)}$ are measured in the intermediate configuration. If the RVE at the lower microscale contains only austenite ($\alpha = 0$) then we have

$$\mathbb{C}^{(0)} = \mathbb{E}^{A}, \tag{27}$$

where the tensor $\mathbb{E}^{A}$ represents the elastic properties of austenite.

For numerical implementations of the model, it is convenient to express the components of $\mathbb{C}^{(\alpha)}$ in the lattice basis of austenite $\{e_i^{A}\}_{i=1}^{3}$ introduced in Section 2.2. To this end, we need the orientations of the lattices of variants β_1 and β_2 in the transformation system α with respect to the lattice of austenite. These can be determined as follows: Let $\hat{e}_i^{(\alpha,\beta_1)}$ and $\hat{e}_i^{(\alpha,\beta_2)}$ be orthonormal unit vectors aligned with the tetragonal axes of the variants β_1 and β_2 *after* the transformation. By convention, set $\hat{e}_{\beta_1}^{(\alpha,\beta_1)}$ and $\hat{e}_{\beta_2}^{(\alpha,\beta_2)}$ to coincide with the c-axis of the tetragonal lattice *after transformation* of variants β_1 and β_2 respectively. Fig. 6 shows a two-dimensional schematic representation of the basis vectors after transformation. Since the transformation deformation gradient related to each variant is given by (6), the variants' basis vectors after transformation, i.e., $\hat{e}_i^{(\alpha,\beta_1)}$ and $\hat{e}_i^{(\alpha,\beta_2)}$, are related to those before transformation, i.e., $e_i^{(\beta_1)}$ and $e_i^{(\beta_2)}$, as follows:

$$\hat{e}_i^{(\alpha,\beta_1)} = \boldsymbol{Q}^{(\alpha,\beta_1)}e_i^{(\beta_1)}, \quad \hat{e}_i^{(\alpha,\beta_2)} = \boldsymbol{Q}^{(\alpha,\beta_2)}e_i^{(\beta_2)}, \tag{28}$$

where, from (9), the rotations are $\boldsymbol{Q}^{(\alpha,\beta_1)} = \bar{\boldsymbol{R}}^{(\alpha)}\boldsymbol{R}^{(\alpha)}$ and $\boldsymbol{Q}^{(\alpha,\beta_2)} = \bar{\boldsymbol{R}}^{(\alpha)}$. The rotations $\boldsymbol{R}^{(\alpha)}$ and $\bar{\boldsymbol{R}}^{(\alpha)}$ can be computed from the algorithm reported by Hane and Shield (1998). Choosing the lattice basis of austenite as a common reference basis, and in view of (2) and (28), the vectors $\hat{e}_i^{(\alpha,\beta_1)}$ and $\hat{e}_i^{(\alpha,\beta_2)}$ can be expressed as

$$\hat{e}_i^{(\alpha,\beta_1)} = \hat{\boldsymbol{Q}}^{(\alpha,\beta_1)}e_i^{A}, \quad \hat{e}_i^{(\alpha,\beta_2)} = \hat{\boldsymbol{Q}}^{(\alpha,\beta_2)}e_i^{A}, \tag{29}$$

with

$$\hat{\boldsymbol{Q}}^{(\alpha,\beta_1)} = \bar{\boldsymbol{R}}^{(\alpha)}\boldsymbol{R}^{(\alpha)}\boldsymbol{R}_{*}^{(\beta_1)}, \quad \hat{\boldsymbol{Q}}^{(\alpha,\beta_2)} = \bar{\boldsymbol{R}}^{(\alpha)}\boldsymbol{R}_{*}^{(\beta_2)}, \tag{30}$$

where the rotations $\boldsymbol{R}_{*}^{(\beta_1)}$ and $\boldsymbol{R}_{*}^{(\beta_2)}$ are given by (3).

The components of $\mathbb{E}^{A}$ with respect to the austenitic tensor basis $\{e_i^{A} \otimes e_j^{A} \otimes e_k^{A} \otimes e_l^{A}\}_{i,j,k,l=1}^{3}$ are denoted as $(E_{ijkl}^{A})_{A}$. For notational convenience, introduce the following convention to express the components of a fourth-order tensor in matrix form: pairs of indices ij or kl are mapped to matrix row I and column J according to

$$ij \mapsto I \quad kl \mapsto J$$
$$11 \to 1, \; 22 \to 2, \; 33 \to 3, \; 23 \to 4, \; 13 \to 5, \; 12 \to 6.$$

With this convention, the components $(E_{ijkl}^{A})_{A}$ of the cubic austenite can be displayed as a 6×6 matrix of components of the form $(E_{IJ}^{A})_{A}$ as follows:

---

[4] We note that the assumption of uniform elastic strain is not in contradiction with the theory of Ball and James (1987), where the stress (and therefore the elastic strain) is taken uniformly as zero in the martensitic variants.
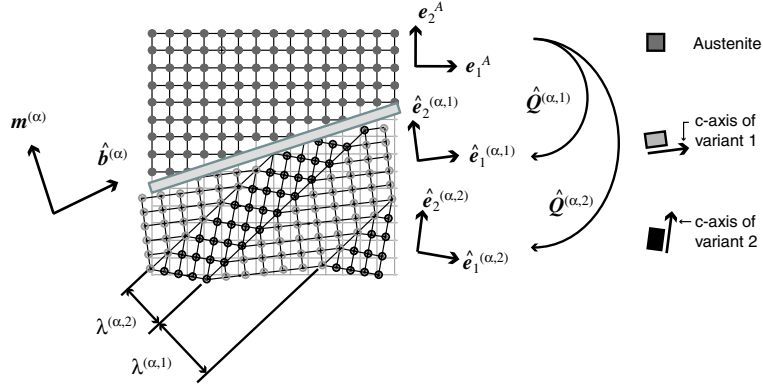
Fig. 6. Two-dimensional schematic representation of the basis vectors $\{\hat{e}_1^{(\alpha,1)}, \hat{e}_2^{(\alpha,1)}\}$ and $\{\hat{e}_1^{(\alpha,2)}, \hat{e}_2^{(\alpha,2)}\}$ of the two tetragonal variants in a transformation system α. By convention, the vector $\hat{e}_\beta^{(\alpha,\beta)}$ is aligned with the c-axis of variant β. The habit plane normal is $\boldsymbol{m}^{(\alpha)}$, the normalized shape vector is $\hat{\boldsymbol{b}}^{(\alpha)}$ and the variants' proportions are $\lambda^{(\alpha,1)}$ and $\lambda^{(\alpha,2)}$.

$$
[\mathbb{E}^A]_A = \begin{pmatrix}
\kappa_1^A & \kappa_2^A & \kappa_2^A & & & \\
\kappa_2^A & \kappa_1^A & \kappa_2^A & & & \\
\kappa_2^A & \kappa_2^A & \kappa_1^A & & & \\
& & & \kappa_3^A & & \\
& & & & \kappa_3^A & \\
& & & & & \kappa_3^A
\end{pmatrix}_A,
\tag{31}
$$

where $\quad \kappa_1^A := (E_{1111}^A)_A = (E_{2222}^A)_A = (E_{3333}^A)_A, \quad \kappa_2^A := (E_{1122}^A)_A = (E_{1133}^A)_A = (E_{2233}^A)_A, \quad \kappa_3^A := (E_{1212}^A)_A = (E_{1313}^A)_A = (E_{2323}^A)_A$ and the other components are found by major and minor symmetry. Components not displayed in the matrix are zero.

The components $(E_{ijkl}^{(\beta_1)})_{(\alpha,\beta_1)}$ and $(E_{ijkl}^{(\beta_2)})_{(\alpha,\beta_2)}$ of the tensors $\mathbb{E}^{(\beta_1)}$ and $\mathbb{E}^{(\beta_2)}$ (stiffness tensors of variants β_1 and β_2 in a system α) are known with respect to the tensor bases $\{\hat{e}_i^{(\alpha,\beta_1)} \otimes \hat{e}_j^{(\alpha,\beta_1)} \otimes \hat{e}_k^{(\alpha,\beta_1)} \otimes \hat{e}_l^{(\alpha,\beta_1)}\}_{i,j,k,l=1}^3$ and $\{\hat{e}_i^{(\alpha,\beta_2)} \otimes \hat{e}_j^{(\alpha,\beta_2)} \otimes \hat{e}_k^{(\alpha,\beta_2)} \otimes \hat{e}_l^{(\alpha,\beta_2)}\}_{i,j,k,l=1}^3$, respectively. Using the previous conventions, the components of each of the tetragonal martensite variants ($\beta = 1, 2, 3$) are as follows:

$$
[\mathbb{E}^{(1)}]_{(\alpha,1)} = \begin{pmatrix}
\kappa_4^M & \kappa_3^M & \kappa_3^M & & & \\
\kappa_3^M & \kappa_1^M & \kappa_2^M & & & \\
\kappa_3^M & \kappa_2^M & \kappa_1^M & & & \\
& & & \kappa_6^M & & \\
& & & & \kappa_5^M & \\
& & & & & \kappa_5^M
\end{pmatrix}_{(\alpha,1)},
\tag{32}
$$

$$
[\mathbb{E}^{(2)}]_{(\alpha,2)} = \begin{pmatrix}
\kappa_1^M & \kappa_3^M & \kappa_2^M & & & \\
\kappa_3^M & \kappa_4^M & \kappa_3^M & & & \\
\kappa_2^M & \kappa_3^M & \kappa_1^M & & & \\
& & & \kappa_5^M & & \\
& & & & \kappa_6^M & \\
& & & & & \kappa_5^M
\end{pmatrix}_{(\alpha,2)},
\tag{33}
$$

$$[\mathbb{E}^{(3)}]_{(\alpha,3)} = \begin{pmatrix} \kappa_1^{\mathrm{M}} & \kappa_2^{\mathrm{M}} & \kappa_3^{\mathrm{M}} & & & \\ \kappa_2^{\mathrm{M}} & \kappa_1^{\mathrm{M}} & \kappa_3^{\mathrm{M}} & & & \\ \kappa_3^{\mathrm{M}} & \kappa_3^{\mathrm{M}} & \kappa_4^{\mathrm{M}} & & & \\ & & & \kappa_5^{\mathrm{M}} & & \\ & & & & \kappa_5^{\mathrm{M}} & \\ & & & & & \kappa_6^{\mathrm{M}} \end{pmatrix}_{(\alpha,3)}, \tag{34}$$

where $\kappa_1^{\mathrm{M}} := (E_{1111}^{(3)})_{(\alpha,3)} = (E_{2222}^{(3)})_{(\alpha,3)}$, $\kappa_2^{\mathrm{M}} := (E_{1122}^{(3)})_{(\alpha,3)}$, $\kappa_3^{\mathrm{M}} = (E_{1133}^{(3)})_{(\alpha,3)} = (E_{2233}^{(3)})_{(\alpha,3)}$, $\kappa_4^{\mathrm{M}} = (E_{3333}^{(3)})_{(\alpha,3)}$, $\kappa_5^{\mathrm{M}} := (E_{1313}^{(3)})_{(\alpha,3)} = (E_{2323}^{(3)})_{(\alpha,3)}$, $\kappa_6^{\mathrm{M}} := (E_{1212}^{(3)})_{(\alpha,3)}$ and the other components are found by major and minor symmetry.

In view of (26), (29) and (30), the components of $\mathbb{C}^{(\alpha)}$ with respect to the austenitic tensor basis are given by

$$(C_{abcd}^{(\alpha)})_{\mathrm{A}} = \lambda^{(\alpha,\beta_1)} \sum_{i,j,k,l=1}^{3} (E_{ijkl}^{(\beta_1)})_{(\alpha,\beta_1)} \hat{Q}_{ai}^{(\alpha,\beta_1)} \hat{Q}_{bj}^{(\alpha,\beta_1)} \hat{Q}_{ck}^{(\alpha,\beta_1)} \hat{Q}_{dl}^{(\alpha,\beta_1)}$$

$$+ \lambda^{(\alpha,\beta_2)} \sum_{i,j,k,l=1}^{3} (E_{ijkl}^{(\beta_2)})_{(\alpha,\beta_2)} \hat{Q}_{ai}^{(\alpha,\beta_2)} \hat{Q}_{bj}^{(\alpha,\beta_2)} \hat{Q}_{ck}^{(\alpha,\beta_2)} \hat{Q}_{dl}^{(\alpha,\beta_2)}, \quad \alpha = 1, \ldots, N, \tag{35}$$

where $\hat{Q}_{ai}^{(\alpha,\beta_1)}$ and $\hat{Q}_{ai}^{(\alpha,\beta_2)}$ are the components of $\hat{\boldsymbol{Q}}^{(\alpha,\beta_1)}$ and $\hat{\boldsymbol{Q}}^{(\alpha,\beta_2)}$.

3.2. Stress and effective stiffness: from upper micro- to mesoscale

We now consider an RVE at the upper microscale as shown in Fig. 2b. To estimate the effective mesoscale elastic properties, we assume that in every point $\boldsymbol{y}^*$ of the subregion $Y_{\boldsymbol{y}}^{(\alpha)}(t)$ the local deformation gradient is equal to the average deformation gradient of that subregion, i.e.,

$$\nabla_{\boldsymbol{y}^*} \hat{\boldsymbol{z}}(\boldsymbol{y}^*, t) = \boldsymbol{F}_{\mathrm{e}}^{(\alpha)} \quad \forall \boldsymbol{y}^* \in Y_{\boldsymbol{y}}^{(\alpha)}(t), \tag{36}$$

where the average elastic deformation gradient $\boldsymbol{F}_{\mathrm{e}}^{(\alpha)}$ is given by (19). We note that the above assumption is strong; however it is used only to estimate the stiffness and it is not part of the general kinematic description formulated in the previous section. In connection with the average elastic deformation gradient $\boldsymbol{F}_{\mathrm{e}}^{(\alpha)}$, we introduce an elastic Green–Lagrange strain in the intermediate configuration, i.e.,

$$\boldsymbol{E}_{\mathrm{e}}^{(\alpha)} := \frac{1}{2}((\boldsymbol{F}_{\mathrm{e}}^{(\alpha)})^{\mathrm{T}} \boldsymbol{F}_{\mathrm{e}}^{(\alpha)} - \boldsymbol{I}). \tag{37}$$

Furthermore, we adopt at the upper microscale a linear relation between the stress and the elastic strain. Thus, the average second Piola–Kirchhoff stress (work conjugate of $\boldsymbol{E}_{\mathrm{e}}^{(\alpha)}$) in each subregion $Y_{\boldsymbol{y}}^{(\alpha)}(t)$ in the intermediate configuration is given by

$$\boldsymbol{S}^{(\alpha)} = \mathbb{C}^{(\alpha)} \boldsymbol{E}_{\mathrm{e}}^{(\alpha)}, \tag{38}$$

where $\mathbb{C}^{(\alpha)}$ is a fourth-order elasticity tensor given by (26) (or by (27) for $\alpha = 0$). We remark that the assumption used to obtain $\mathbb{C}^{(\alpha)}$ in (26) (i.e., uniform elastic strain in each martensitic variant) is consistent with (36). Let $\boldsymbol{S} = \boldsymbol{S}(\boldsymbol{y}, t)$ be the second Piola–Kirchhoff stress in the intermediate configuration at the mesoscale. The tensor $\boldsymbol{S}$ can be computed as the volume average of the tensors $\boldsymbol{S}^{(\alpha)}$, which, in view of (38), can be expressed as

$$S(y,t) = \frac{1}{|Y_y|} \sum_{\alpha=0}^{N} |Y_y^{(\alpha)}(t)| S^{(\alpha)} = \frac{1}{|Y_y|} \sum_{\alpha=0}^{N} |Y_y^{(\alpha)}(t)| \mathbb{C}^{(\alpha)} E_e^{(\alpha)}. \tag{39}$$

Combining (37) and (39) with the kinematic assumption (22) provides the second Piola–Kirchhoff stress in the intermediate configuration at the mesoscale, i.e.,

$$S = \mathbb{C} E_e, \tag{40}$$

where the elastic Green–Lagrange strain at the mesoscale is defined as

$$E_e := \frac{1}{2}(F_e^T F_e - I), \tag{41}$$

and the effective properties $\mathbb{C}$ are given by

$$\mathbb{C} = \sum_{\alpha=0}^{N} \varphi^{(\alpha)} \mathbb{C}^{(\alpha)}, \quad \varphi^{(\alpha)} := \frac{|Y_y^{(\alpha)}(t)|}{|Y_y|}. \tag{42}$$

The ratio $\varphi^{(\alpha)} = |Y_y^{(\alpha)}(t)|/|Y_y|$ represents the volume fraction of the transformation system α in the intermediate configuration. To obtain a formula that involves the volume fractions $\xi^{(\alpha)}$ defined in (20), we first note that,

$$\varphi^{(\alpha)} = \frac{|Y_y^{(\alpha)}(t)|}{|Y_y|} = \frac{\det F_{tr}^{(\alpha)}}{\det F_{tr}} \xi^{(\alpha)}, \tag{43}$$

where $F_{tr}^{(\alpha)}$ is given by (10) and F_{tr} by (24). Following Ball and James (1987), one can show that for all transformation systems $\alpha = 1, \ldots, N$, the volumetric change δ_T due to transformation is the same, i.e., by (10) and (11),

$$\det F_{tr}^{(\alpha)} = 1 + \delta_T \quad \text{with} \quad \delta_T := b^{(\alpha)} \cdot m^{(\alpha)}. \tag{44}$$

For $\alpha = 0$ (austenite), we have $\det F_{tr}^{(0)} = 1$. To guarantee that the volume fractions $\varphi^{(\alpha)}$ in the intermediate configuration satisfy the relation $\sum_{\alpha=0}^{N} \varphi^{(\alpha)} = 1$, and in view of (10), (11), (21), (43) and (44), the Jacobian J_{tr} of the transformation deformation gradient F_{tr} is approximated as follows:

$$J_{tr} := \det F_{tr} \approx 1 + (1 - \xi^{(0)})\delta_T. \tag{45}$$

Alternatively, the approximation on the right side of (45) can be obtained by a direct calculation of J_{tr} where the non-linear terms in the volume fractions can be neglected since they remain small over the entire range $0 \leqslant \xi^{(0)} \leqslant 1$ for typical values of δ_T and γ_T. From (21), (42)–(44) it follows that the effective stiffness at the mesoscale is

$$\mathbb{C} = \frac{1}{J_{tr}} \xi^{(0)} \mathbb{C}^{(0)} + \sum_{\alpha=1}^{N} \left(\frac{1+\delta_T}{J_{tr}}\right) \xi^{(\alpha)} \mathbb{C}^{(\alpha)} = \frac{1}{J_{tr}} \left\{ \left(1 - \sum_{\alpha=1}^{N} \xi^{(\alpha)}\right) \mathbb{C}^A + (1+\delta_T) \sum_{\alpha=1}^{N} \xi^{(\alpha)} \mathbb{C}^{(\alpha)} \right\}, \tag{46}$$

where we set $\mathbb{C}^A := \mathbb{C}^{(0)}$ as the elastic properties of the austenite given in (27). Note that for the special case where the properties of the martensite are equal to those of austenite, i.e., $\mathbb{C}^{(\alpha)} = \mathbb{C}^A$, the approximation (45) guarantees that the effective stiffness is equal to $\mathbb{C}^A$. Although the averaging scheme used here for deriving the elastic properties is straightforward (i.e., uniform elastic deformation), we note that in the above procedure we incorporate two effects that are commonly neglected in martensitic transformation models: (i) the tensor $\mathbb{C}$ preserves information at the mesoscale regarding the proportion and orientation of the individual martensitic variants for each transformation system α and (ii) the tensor $\mathbb{C}$ incorporates the influence of volumetric changes due to the transformation when the volume fractions are measured in the reference configuration.

4. Thermodynamic formulation

The transformation from austenite to martensite is a thermodynamically irreversible process since energy is dissipated during transformation. To complete the transformation model, we introduce the thermal variables and balance principles and we derive an expression for the dissipation where the influence of the transformation systems is explicitly taken into account. In addition, the evolution of the transformation deformation gradient F_{tr} needs to be determined. As we shall see in this section, both the evolution of F_{tr} and the dissipation depend on a quantity known as the *transformation driving force*.

Following the formalism proposed by Onsager for irreversible thermodynamics (see, e.g., Callen, 1985), for each physical phenomenon "k" where energy is dissipated, a pair of conjugate quantities can be identified, termed generically *affinities* $\mathscr{F}_k$ and *fluxes* $\mathscr{J}_k$. The corresponding contribution to the dissipation is equal to the product $\mathscr{F}_k \mathscr{J}_k$. Furthermore, a relation between $\mathscr{F}_k$ and $\mathscr{J}_k$ is required in order to fully characterize the constitutive behavior of a material. For phase transformations, the driving force is an affinity and its constitutive connection to the corresponding flux is known as a *kinetic relation*. Mesoscale kinetic relations can in principle be obtained by homogenization of microscale kinetic laws. Bhattacharya (1999) homogenized a kinetic law for a one-dimensional model of a material undergoing a phase transformation. However, in a three-dimensional setting the homogenization procedure is complex and still a rather open problem. Thus, for simplicity, we propose a kinetic relation *directly* at the mesoscale. From the thermodynamic framework presented in this section we will identify the conjugated variables that characterize the mesoscale kinetic law and its specification will be given in Section 5.

4.1. Thermodynamic quantities

We introduce the following thermal quantities defined in the *reference* configuration: let θ be the (absolute) temperature, η the entropy density per unit mass, q the heat flux per unit area and r the body heat source per unit volume. In addition, let Φ be the entropy flux per unit area and s the entropy source per unit volume, given by (Liu, 2002)

$$\Phi = \frac{q}{\theta}, \quad s = \frac{r}{\theta}. \tag{47}$$

In analogy with the kinematic relations (12) and (24), we introduce equivalent expressions for the entropy density. Materials can coexist in two different phases at the same temperature but at different entropies (see, e.g., Callen, 1985). The analogous situation for mechanical fields is that two different phases of a material can coexist at the same stress but with different deformation gradients. Hence, within a thermodynamic framework the entropy density has a similar role as the deformation gradient, while the temperature is analogous to the stress. In analogy with the entropy decomposition used by Simo and Miehe (1992) for thermoplastic behavior, we propose the following decomposition of the total entropy density:

$$\eta = \eta_e + \eta_{tr}, \tag{48}$$

where η_e represents the conservative part of the entropy density and η_{tr} is the *transformation entropy density*. In order to provide an expression for η_{tr}, we define the *transformation temperature* θ_T as the temperature at which austenite can transform isothermally into a specific system α of martensite at zero stress, *without dissipation* and in the *absence* of an internal energy barrier. We remark that in metals and alloys the actual temperature at which transformation occurs is usually different from θ_T, as a result of the presence of an internal energy barrier. Furthermore, define the *latent heat* $\lambda_T^{(\alpha)}$ of system α *at* the transformation temperature θ_T and *at* zero stress as the heat required per unit mass during a complete transformation from austenite to system α of martensite. Consistent with the definition of $\lambda_T^{(\alpha)}$, we propose the following expression for the transformation entropy density:

$$\eta_{\text{tr}} := \sum_{\alpha=1}^{N} \xi^{(\alpha)} \frac{\lambda_{\text{T}}^{(\alpha)}}{\theta_{\text{T}}}. \tag{49}$$

Eqs. (48) and (49) are the thermal analogues of (12) and (24) respectively. The transformation entropy η_{tr} represents the entropy change as $\xi^{(\alpha)}$ changes during an isothermal phase transformation at the transformation temperature (and at zero stress). The analogous situation in the mechanical framework is that $\boldsymbol{F}_{\text{tr}}$ measures changes in $\boldsymbol{F}$ only *at* zero stress (and at the transformation temperature). Since the entropy of austenite (high-temperature phase) is higher than the entropy of martensite (low-temperature phase), $\lambda_{\text{T}}^{(\alpha)}$ in (49) is *negative*. We note that the latent heat at temperatures other than θ_{T} needs to include changes in η_{e} as well.[5]

4.2. Thermodynamic restrictions and transformation driving force

In their work on propagating phase boundaries, Abeyaratne and Knowles (1991) identified the velocity of an interface as a flux. By analogy, a natural choice at the mesoscopic level for the flux $\mathcal{J}_{\text{tr}}^{(\alpha)}$, associated to a phase transformation from austenite to system α of martensite, is the time rate of change of the volume fraction $\dot{\xi}^{(\alpha)}$ of the region occupied by the transformation system α. The corresponding affinity (i.e., the transformation driving force, henceforth denoted as $f^{(\alpha)}$) can be identified from the expression for dissipation following Onsager's approach. In addition, for heat conduction, the flux is the entropy flux (i.e., $\mathcal{J}_q = \boldsymbol{\Phi}$) and, as shown below, the corresponding affinity is (minus) the temperature gradient (i.e., $\mathcal{F}_q = -\nabla\theta$). In this section we derive an expression for the dissipation and subsequently use the second law of thermodynamics in order to obtain constitutive restrictions and a *definition* for the driving force $f^{(\alpha)}$.

Let ϵ be the internal energy density per unit mass,[6] $\boldsymbol{P}$ the first Piola–Kirchhoff stress in the reference configuration, $\boldsymbol{b}_f$ the body force per unit reference volume, ρ_0 the mass density in the reference configuration and $\boldsymbol{a}$ the acceleration of a material point $\boldsymbol{x}$. Assuming that all field quantities at the mesoscale are continuously differentiable, the balance of linear momentum, localized per unit reference volume, is given by

$$\text{div}\,\boldsymbol{P} + \boldsymbol{b}_f = \rho_0 \boldsymbol{a}.$$

The balance of total energy, combined with the balance of linear momentum and localized per unit reference volume, can be expressed as

$$\rho_0 \dot{\epsilon} + (\text{div}\,\boldsymbol{q} - r) - \boldsymbol{P} \cdot \dot{\boldsymbol{F}} = 0, \tag{50}$$

where the term $\boldsymbol{P} \cdot \dot{\boldsymbol{F}}$ represents the *internal power*. The entropy rate Γ per unit referential volume is

$$\Gamma := \rho_0 \dot{\eta} + (\text{div}\,\boldsymbol{\Phi} - s) = \rho_0 \dot{\eta} + \frac{1}{\theta}(\text{div}\,\boldsymbol{q} - r) - \frac{1}{\theta^2}\boldsymbol{q} \cdot \nabla\theta, \tag{51}$$

where we have used (47). Defining the total *dissipation density* $\mathcal{D}$ per unit reference volume as

$$\mathcal{D} := \Gamma\theta \tag{52}$$

and combining it with (47), (50) and (51), the dissipation can be expressed as

$$\mathcal{D} = -\rho_0 \dot{\epsilon} + \rho_0 \theta \dot{\eta} + \boldsymbol{P} \cdot \dot{\boldsymbol{F}} - \nabla\theta \cdot \boldsymbol{\Phi}. \tag{53}$$

---

[5] A specific expression will be shown at the end of Section 5.3.

[6] All energy densities as well as the entropy density are defined here per unit mass and not per unit volume, as often encountered in the literature. The advantage of the present choice is that otherwise we need to define one such density per configuration.

With the goal of deriving an expression for the transformation driving force, we analyze each term in (53) in more detail. Using the kinematic assumptions in equations (12) and (24), we may express the internal power as

$$\boldsymbol{P} \cdot \dot{\boldsymbol{F}} = \boldsymbol{P}\boldsymbol{F}_{\mathrm{tr}}^{\mathrm{T}} \cdot \dot{\boldsymbol{F}}_{\mathrm{e}} + \sum_{\alpha=1}^{N} \tau_m^{(\alpha)} \dot{\xi}^{(\alpha)}, \tag{54}$$

where $\tau_m^{(\alpha)}$ is given by

$$\tau_m^{(\alpha)} := \boldsymbol{F}_{\mathrm{e}}^{\mathrm{T}} \boldsymbol{P} \cdot \boldsymbol{\gamma}^{(\alpha)}, \quad \alpha = 1, \dots, N \tag{55}$$

and is referred to as the *resolved stress* for the transformation system α. We note that the thermal deformation gradient has been neglected (i.e., $\boldsymbol{F}_{\mathrm{th}} \simeq \boldsymbol{I}$ in the decomposition (12)) and therefore does not appear in (54). From (48) and (49) it follows that the second term in (53) is

$$\rho_0 \theta \dot{\eta} = \rho_0 \theta \dot{\eta}_{\mathrm{e}} + \sum_{\alpha=1}^{N} \tau_{\mathrm{th}}^{(\alpha)} \dot{\xi}^{(\alpha)}, \tag{56}$$

where $\tau_{\mathrm{th}}^{(\alpha)}$ is given by

$$\tau_{\mathrm{th}}^{(\alpha)} := \rho_0 \theta \frac{\lambda_{\mathrm{T}}^{(\alpha)}}{\theta_{\mathrm{T}}}, \quad \alpha = 1, \dots, N \tag{57}$$

and can be interpreted as the thermal analogue of the resolved stress $\tau_m^{(\alpha)}$ given in (55).

We now turn our attention to the internal energy density ϵ, and its time derivative appearing in (53). We propose as mesoscopic state variables the elastic deformation gradient $\boldsymbol{F}_{\mathrm{e}}$, the conservative part of the entropy density η_{e} and the volume fractions $\xi^{(\alpha)}$ of the transformation systems $\alpha = 1, \dots, N$. In view of (12), (24), (48) and (49), it is also possible to use $\boldsymbol{F}$ and η as variables for the internal energy density; however in that case the expression for the internal energy becomes cumbersome. As mentioned previously, the dissipative behavior is characterized by relations between affinities and fluxes. In the present model, the fluxes are $\dot{\xi}^{(\alpha)}$ and $\boldsymbol{\Phi}$. The classical procedure is to include all variables in all constitutive assumptions without a priori discarding any of them. Consequently, we assume that the internal energy density depends, in addition to the state variables, on the fluxes $\dot{\xi}^{(\alpha)}$ and $\boldsymbol{\Phi}$, i.e.,

$$\epsilon = \bar{\epsilon}(\boldsymbol{F}_{\mathrm{e}}, \eta_{\mathrm{e}}, \boldsymbol{\xi}; \dot{\boldsymbol{\xi}}, \boldsymbol{\Phi}), \tag{58}$$

where, for notational convenience, we use a semi-colon to distinguish the state variables from the fluxes. Further, we have collected the volume fractions $\xi^{(\alpha)}$, with $\alpha = 1, \dots, N$, in a vector ξ as follows:

$$\boldsymbol{\xi} := \{\xi^{(1)}, \dots, \xi^{(N)}\}.$$

In addition to the internal energy ϵ, the dependent variables are the first Piola–Kirchhoff stress in the reference configuration $\boldsymbol{P}$, the temperature θ and the affinities $\mathscr{F}_q$ and $\mathscr{F}_{\mathrm{tr}}^{(\alpha)}$ associated with heat conduction and phase transformations respectively. We recall that these affinities are (minus) the temperature gradient $-\nabla\theta$ and the transformation driving force $f^{(\alpha)}$, respectively, as introduced at the beginning of this section. Consistent with the assumption (58), we suppose that *all* dependent variables (i.e., $\boldsymbol{P}$, θ, $-\nabla\theta$ and $f^{(\alpha)}$) depend on *all* the independent variables (i.e., $\boldsymbol{F}_{\mathrm{e}}, \eta_{\mathrm{e}}, \boldsymbol{\xi}, \dot{\boldsymbol{\xi}}$ and $\boldsymbol{\Phi}$).

Combining (53), (54), (56) and (58), the dissipation density can be expressed as

$$\mathscr{D} = \left(\boldsymbol{P}\boldsymbol{F}_{\mathrm{tr}}^{\mathrm{T}} - \rho_0 \frac{\partial\bar{\epsilon}}{\partial\boldsymbol{F}_{\mathrm{e}}}\right) \cdot \dot{\boldsymbol{F}}_{\mathrm{e}} + \rho_0 \left(\theta - \frac{\partial\bar{\epsilon}}{\partial\eta_{\mathrm{e}}}\right) \dot{\eta}_{\mathrm{e}} + \sum_{\alpha=1}^{N} \left(\tau_m^{(\alpha)} + \tau_{\mathrm{th}}^{(\alpha)} - \rho_0 \frac{\partial\bar{\epsilon}}{\partial\xi^{(\alpha)}}\right) \dot{\xi}^{(\alpha)} - \nabla\theta \cdot \boldsymbol{\Phi}$$

$$- \sum_{\alpha=1}^{N} \rho_0 \left(\frac{\partial\bar{\epsilon}}{\partial\dot{\xi}^{(\alpha)}}\right) \ddot{\xi}^{(\alpha)} - \rho_0 \frac{\partial\bar{\epsilon}}{\partial\boldsymbol{\Phi}} \cdot \dot{\boldsymbol{\Phi}}. \tag{59}$$

The second law of thermodynamics, in the form of the Clausius-Duhem inequality, indicates that in any thermomechanical process the entropy rate density is non-negative, i.e., $\Gamma \geqslant 0$. Since $\Gamma = \mathscr{D}/\theta$ and $\theta > 0$, this is equivalent to

$$\mathscr{D} \geqslant 0,$$

which is the *dissipation inequality*. Following the procedure of Coleman and Noll (1963), the terms in (59) that are multiplied by the rates $\dot{\boldsymbol{F}}_e$, $\dot{\eta}_e$, $\ddot{\boldsymbol{\xi}}$ and $\dot{\boldsymbol{\Phi}}$ must vanish. This follows from the assumption that these terms do not depend on the corresponding rates and the fact that, if these terms were not equal to zero, one could specify a process where the dissipation is negative. Consequently, it follows that

$$\boldsymbol{P} = \rho_0 \frac{\partial \bar{\epsilon}}{\partial \boldsymbol{F}_e} \boldsymbol{F}_{tr}^{-T}, \quad \theta = \frac{\partial \bar{\epsilon}}{\partial \eta_e} \tag{60}$$

and that the internal energy density does not depend on the fluxes $\dot{\boldsymbol{\xi}}$ or $\boldsymbol{\Phi}$, which reduces (58) to

$$\epsilon = \bar{\epsilon}(\boldsymbol{F}_e, \eta_e, \boldsymbol{\xi}). \tag{61}$$

In (61), we use the same symbol $\bar{\epsilon}$ as in (58) to denote the internal energy density, although henceforth we only view it as a function of the state variables $\boldsymbol{F}_e$, η_e and $\boldsymbol{\xi}$.

The remaining non-zero terms in (59) correspond to the dissipation due to heat conduction, i.e.,

$$\mathscr{D}_q := -\nabla\theta \cdot \boldsymbol{\Phi} \tag{62}$$

and the dissipation due to the phase transformation, i.e.,

$$\mathscr{D}_{tr} := \sum_{\alpha=1}^{N} f^{(\alpha)} \dot{\xi}^{(\alpha)}, \tag{63}$$

where

$$f^{(\alpha)} := \tau_m^{(\alpha)} + \tau_{th}^{(\alpha)} - \rho_0 \frac{\partial \bar{\epsilon}}{\partial \xi^{(\alpha)}}. \tag{64}$$

Following the terminology of Onsager (see also Abeyaratne and Knowles (1990) for the specific case of phase transformations), the transformation dissipation density in (63) is identified as a product of an affinity times a flux. The affinity $f^{(\alpha)}$ is interpreted as the *transformation driving force* of the corresponding transformation system α. From (62), we confirm that for heat conduction the affinity is $-\nabla\theta$ and the flux is $\boldsymbol{\Phi}$.

From (59), (60), (62) and (63), the dissipation inequality can be written as

$$\mathscr{D} = \mathscr{D}_q + \mathscr{D}_{tr} \geqslant 0. \tag{65}$$

However, it is assumed that the inequalities $\mathscr{D}_{tr} \geqslant 0$ and $\mathscr{D}_q \geqslant 0$ hold *independently* of each other, and thus

$$\mathscr{D}_{tr} = \sum_{\alpha=1}^{N} f^{(\alpha)} \dot{\xi}^{(\alpha)} \geqslant 0. \tag{66}$$

A posteriori, to motivate the choice of state variables and fluxes, we observe that, had we not assumed that $f^{(\alpha)}$ depends on $\dot{\xi}^{(\alpha)}$, then necessarily $f^{(\alpha)}$ would have been zero and the model would have predicted a dissipation-free transformation.

It is important to note that the definition of the driving force given in (64) is not in contradiction with classical definitions of thermodynamically conjugated quantities. In particular, $f^{(\alpha)}$ could be defined as (minus) the derivative of the internal energy with respect to $\xi^{(\alpha)}$ (Rice, 1971, Eq. (8)). According to (64) this might not be immediately evident. However, it should be pointed out that in the above definition the total deformation gradient $\boldsymbol{F}$ and the total entropy density η are taken as variables for the internal energy density (instead of $\boldsymbol{F}_e$ and η_e as in (61)). If we consider a process where the total deformation gradient and the total

entropy density are held fixed, say $F = F_0$ and $\eta = \eta_0$, then, from (12), (24), (48) and (49), we can determine the required change in F_e and η_e with respect to $\xi^{(\alpha)}$ such that F and η are held constant, i.e., since

$$\frac{\partial F_0}{\partial \xi^{(\alpha)}} = \frac{\partial F_e}{\partial \xi^{(\alpha)}}\bigg|_{F_0} F_{tr} + F_e \gamma^{(\alpha)} = \mathbf{0}, \quad \frac{\partial \eta_0}{\partial \xi^{(\alpha)}} = \frac{\partial \eta_e}{\partial \xi^{(\alpha)}}\bigg|_{\eta_0} + \frac{\lambda_T^{(\alpha)}}{\theta_T} = 0,$$

then

$$\frac{\partial F_e}{\partial \xi^{(\alpha)}}\bigg|_{F_0} = -F_e \gamma^{(\alpha)} F_{tr}^{-1}, \quad \frac{\partial \eta_e}{\partial \xi^{(\alpha)}}\bigg|_{\eta_0} = -\frac{\lambda_T^{(\alpha)}}{\theta_T}. \tag{67}$$

From (55), (57), (60), (61), (64) and (67) it follows that

$$f^{(\alpha)} = -\rho_0 \frac{\partial \bar{\epsilon}}{\partial \xi^{(\alpha)}}\bigg|_{F_0, \eta_0}, \tag{68}$$

a result that is equivalent to (64). However, since we find it conceptually more advantageous to work with F_e and η_e as variables for the energy density, we view (68) as a result rather than a definition. In the next subsection we will provide additional relations between $f^{(\alpha)}$ and other thermodynamic energies.

4.3. Formulation in terms of the Helmholtz and Gibbs energy densities

For mechanics problems it is convenient to work with the Helmholtz energy density ψ instead of the internal energy density ϵ since the temperature is viewed as an experimentally more manageable and intuitively more accessible variable than the entropy. The Helmholtz energy is the potential that uses F_e, θ and ξ as independent variables. Similarly, some researchers find it convenient to work with Gibbs' energy, which is the potential that uses P, θ and ξ as natural variables. We provide in this section some useful relations in terms of these potentials.

The Helmholtz energy density can be obtained from the internal energy density by means of a Legendre transformation,[7] i.e.,

$$\bar{\psi}(F_e, \theta, \xi) = \bar{\epsilon}(F_e, \tilde{\eta}_e(F_e, \theta, \xi), \xi) - \theta \tilde{\eta}_e(F_e, \theta, \xi), \tag{69}$$

where the function $\tilde{\eta}_e$ is formally obtained by combining the second relation in (60) with (61) and solving for η_e in terms of θ. From (69) and the second relation in (60), it follows that:

$$\frac{\partial \bar{\psi}}{\partial F_e} = \frac{\partial \bar{\epsilon}}{\partial F_e}, \quad \eta_e = -\frac{\partial \bar{\psi}}{\partial \theta}, \quad \frac{\partial \bar{\psi}}{\partial \xi} = \frac{\partial \bar{\epsilon}}{\partial \xi}, \tag{70}$$

where the partial derivatives of each energy density are computed while holding the corresponding natural variables fixed (i.e., (F_e, θ, ξ) for $\bar{\psi}$ and (F_e, η_e, ξ) for $\bar{\epsilon}$).

We note that a restriction on the form of the Helmholtz energy density (which also applies to $\bar{\epsilon}$) is provided by the principle of material frame indifference. In particular, the Helmholtz energy density cannot depend on the full elastic deformation gradient but rather on a strain measure based on the stretch part only. One such measure is the elastic Green–Lagrange strain E_e. Consequently, we consider a function $\hat{\psi}$ such that

$$\hat{\psi}(E_e, \theta, \xi) = \bar{\psi}(F_e, \theta, \xi), \tag{71}$$

---

[7] Observe that on the right hand side of (69) we use the product $\theta \eta_e$ (instead of the more classical expression $\theta \eta$) in accordance with the choice of variables of $\bar{\psi}$ and $\bar{\epsilon}$.

where E_e and F_e are related via (41). In view of constructing a specific model for the material, we will work with the Helmholtz energy density $\hat{\psi}$ and, therefore, it is useful to establish relations for the partial derivatives of this energy. We observe from (71) that derivatives of $\hat{\psi}$ with respect to θ or ξ are the same as the derivatives of $\bar{\psi}$ with respect to those variables. In particular, from the second relation in (70), we have

$$\eta_e = -\frac{\partial \hat{\psi}}{\partial \theta} \tag{72}$$

and, from (64), we may express the driving force in terms of $\hat{\psi}$ as

$$f^{(\alpha)} = \tau_m^{(\alpha)} + \tau_{th}^{(\alpha)} - \rho_0 \frac{\partial \hat{\psi}}{\partial \xi^{(\alpha)}}. \tag{73}$$

Finally, for subsequent use, we establish a connection between the second Piola–Kirchhoff stress S in the intermediate configuration and the Helmholtz energy density $\hat{\psi}$. Using the chain rule and the symmetry of E_e, it follows from (71) that

$$\frac{\partial \bar{\psi}}{\partial F_e} = F_e \frac{\partial \hat{\psi}}{\partial E_e}. \tag{74}$$

Let

$$J := \det F = J_e J_{tr} \tag{75}$$

be the Jacobian of the total deformation, where

$$J_e := \det F_e \tag{76}$$

and J_{tr} is defined in (45). The mass densities $\tilde{\rho}$ and ρ in the intermediate and current configurations are related to the mass density ρ_0 in the reference configuration via

$$\tilde{\rho} = \frac{\rho_0}{J_{tr}}, \quad \rho = \frac{\rho_0}{J}. \tag{77}$$

The first Piola–Kirchhoff stress P in the reference configuration is related by definition to the second Piola–Kirchhoff stress S in the intermediate configuration as

$$P = J_{tr} F_e S F_{tr}^{-T}. \tag{78}$$

Consequently, in view of (60), (70), (74), (77) and (78), it follows that:

$$S = \tilde{\rho} \frac{\partial \hat{\psi}}{\partial E_e}. \tag{79}$$

In order to compare the present formulation with other theories, we list a series of relations that include Gibbs' energy since it is often used in the study of phase transformations, particularly in the definition of the driving force. The Gibbs' energy density $\bar{g}$ (per unit mass) uses P, θ and ξ as natural variables. It can be constructed via a Legendre transformation of the Helmholtz energy density with respect to the conjugate pair $(F_e, \rho_0^{-1} P F_{tr}^T)$[8] or, equivalently, as a Legendre transformation of the internal energy density with respect to the conjugate pairs (η_e, θ) and $(F_e, \rho_0^{-1} P F_{tr}^T)$, i.e.,

$$\bar{g} = \bar{\psi} - \frac{1}{\rho_0} F_e \cdot P F_{tr}^T = \bar{\epsilon} - \eta_e \theta - \frac{1}{\rho_0} F_e \cdot P F_{tr}^T, \tag{80}$$

---

[8] This conjugate pair is obtained from (60). For definiteness we have opted for this pair but it is also possible to work with $(E_e, \tilde{\rho}^{-1} S)$ and functions $\hat{g}$, $\hat{\psi}$ and $\hat{\epsilon}$.

where, for ease of notation, we have omitted the arguments of $\boldsymbol{F}_e$, η_e and the energies, although they should be interpreted as explicit or implicit functions of $\boldsymbol{P}$, θ and $\boldsymbol{\xi}$. A direct calculation that utilizes (24), (55), (60), (70) and (80) gives

$$\boldsymbol{F}_e = -\rho_0 \frac{\partial \bar{g}}{\partial \boldsymbol{P}} \boldsymbol{F}_{\mathrm{tr}}^{-1}, \quad \eta_e = -\frac{\partial \bar{g}}{\partial \theta}, \quad \frac{\partial \bar{g}}{\partial \xi^{(\alpha)}} = \frac{\partial \bar{\psi}}{\partial \xi^{(\alpha)}} - \frac{1}{\rho_0} \tau_m^{(\alpha)}, \tag{81}$$

where the partial derivatives are taken while holding the natural variables fixed for each energy density. We note that, from the third relation in (81) and in view of (71) and (73), the relation between the driving force and the Gibbs' energy density is

$$f^{(\alpha)} = \tau_{\mathrm{th}}^{(\alpha)} - \rho_0 \frac{\partial \bar{g}}{\partial \xi^{(\alpha)}}, \tag{82}$$

with $\tau_{\mathrm{th}}^{(\alpha)}$ given by (57). The transformation driving force is often defined in the materials science literature as (minus) the change in Gibbs' energy as the material transforms from one phase to another. We observe that the driving force in (82) does not conform to that definition. However, this is related to the fact that θ and η_e are taken as conjugate variables in the Gibbs' energy density (see the second equation in (81)), instead of the commonly used combination of θ and total entropy η. Consequently, the effect of the transformation entropy η_{tr} on the driving force $f^{(\alpha)}$ is represented in (82) by the additional term $\tau_{\mathrm{th}}^{(\alpha)}$.

5. Thermomechanical constitutive model

In order to derive an expression for the driving force, a specific form of the Helmholtz energy $\hat{\psi}$ is required in (73). To obtain the strain energy contribution to the Helmholtz energy, we integrate the stress-strain relation (40) with respect to $\boldsymbol{E}_e$. Similarly, to determine the thermal energy contribution, an entropy-temperature relation is adopted and integrated with respect to θ. Additionally, we propose a form for the surface energy that depends on $\boldsymbol{\xi}$. With this form of the Helmholtz energy, we use (73) in order to compute the driving force $f^{(\alpha)}$. A specific kinetic relation is then proposed to describe the evolution of the martensitic volume fractions.

5.1. Helmholtz energy density for austenite

As shown in (71), the function $\hat{\psi}$ depends on $\boldsymbol{E}_e$, θ and $\boldsymbol{\xi}$. We start with the strain energy part of the Helmholtz energy density using the results derived in Section 2. From (40), (77) and (79), the derivative of the Helmholtz energy density with respect to the elastic Green–Lagrange strain is given by

$$\frac{\partial \hat{\psi}}{\partial \boldsymbol{E}_e} = \frac{J_{\mathrm{tr}}}{\rho_0} \mathbb{C} \boldsymbol{E}_e. \tag{83}$$

Integrating $\hat{\psi}$ with respect to $\boldsymbol{E}_e$, keeping in mind that neither J_{tr} nor $\mathbb{C}$ depends on $\boldsymbol{E}_e$, it follows that

$$\hat{\psi}(\boldsymbol{E}_e, \theta, \boldsymbol{\xi}) = \psi_m(\boldsymbol{E}_e, \boldsymbol{\xi}) + \psi_1(\theta, \boldsymbol{\xi}), \tag{84}$$

where

$$\psi_m(\boldsymbol{E}_e, \boldsymbol{\xi}) := \frac{J_{\mathrm{tr}}(\boldsymbol{\xi})}{2\rho_0} \mathbb{C}(\boldsymbol{\xi}) \boldsymbol{E}_e \cdot \boldsymbol{E}_e \tag{85}$$

is the (bulk) elastic strain energy density and ψ_1 represents the terms of the Helmholtz energy density that are not part of the elastic strain energy density (i.e., the integration constants). Note that both J_{tr} and $\mathbb{C}$ depend explicitly on ξ, which reflects a coupling between the transformation and elastic behavior.

We develop an approximation to the thermal part of the energy using a similar approach as for the strain energy density. As in Section 3.2, consider a mesoscopic RVE with subregions $Y_y^{(\alpha)}(t)$. In each subregion we have a uniform temperature $\theta^{(\alpha)}$ and a corresponding entropy $\eta_e^{(\alpha)}$. The specific heat capacity per unit mass, measured at constant elastic deformation for each phase $\alpha = 0, \ldots, N$, is defined as $h^{(\alpha)} := \theta^{(\alpha)} \partial \eta_e^{(\alpha)} / \partial \theta^{(\alpha)}$. We assume that $h^{(\alpha)}$ does not depend on the temperature, therefore we use the following constitutive relation for the conservative entropy density in terms of the temperature:

$$\eta_e^{(\alpha)} = h^{(\alpha)} \ln \frac{\theta^{(\alpha)}}{\theta_T} + \eta_T, \tag{86}$$

where η_T is the common value of $\eta_e^{(\alpha)}$ at the transformation temperature for all systems α. We note that the above entropy-temperature constitutive relation is only valid for a temperature range where $\eta_e^{(\alpha)}$ is positive.

The mesoscopic entropy density η_e is obtained by averaging the entropies in an RVE in the intermediate configuration centered at a point y (see Fig. 5), i.e.,

$$\tilde{\rho}(y,t)\eta_e(y,t) = \frac{1}{|Y_y|} \sum_{\alpha=0}^{N} \int_{Y_y^{(\alpha)}(t)} \tilde{\rho}^{(\alpha)}(y^*,t)\eta_e^{(\alpha)}(y^*,t)\, dv_{y^*}, \tag{87}$$

where $\tilde{\rho}$ is the mass density in the intermediate configuration defined in (77) and

$$\tilde{\rho}^{(\alpha)} := \frac{\rho_0}{J_{tr}^{(\alpha)}}, \tag{88}$$

with $J_{tr}^{(\alpha)}$ as in (17). An *effective* specific heat capacity per unit mass can be obtained assuming all subregions to have the same temperature $\theta^{(\alpha)} = \theta$. If we define the effective heat capacity h such that

$$\eta_e = h \ln \frac{\theta}{\theta_T} + \eta_T, \tag{89}$$

then, in view of (21), (43), (45), (77), (86), (87) and (88), h is given by

$$h(\xi) = \left(1 - \sum_{\alpha=1}^{N} \xi^{(\alpha)}\right) h^A + \sum_{\alpha=1}^{N} \xi^{(\alpha)} h^{(\alpha)}, \tag{90}$$

where $h^A := h^{(0)}$ is the specific heat of austenite.

With the constitutive model (89) and in view of (72), we have

$$\frac{\partial \hat{\psi}}{\partial \theta} = -h \ln \frac{\theta}{\theta_T} - \eta_T. \tag{91}$$

Integration of (91) with respect to the temperature provides the following expression for the Helmholtz energy density:

$$\hat{\psi}(E_e, \theta, \xi) = \psi_{th}(\theta, \xi) + \psi_2(E_e, \xi), \tag{92}$$

where ψ_{th} is the thermal energy given by

$$\psi_{th}(\theta, \xi) := -h(\xi)\theta \ln \frac{\theta}{\theta_T} + (h(\xi) - \eta_T)\theta, \tag{93}$$

and ψ_2 corresponds to the terms of the Helmholtz energy that are not part of the thermal energy.

At this point we have two equivalent expressions for the Helmholtz energy, namely (84) and (92). Differentiating these expressions with respect to $\boldsymbol{E}_e$ and θ gives

$$\frac{\partial \psi_m}{\partial \boldsymbol{E}_e} + \frac{\partial \psi_1}{\partial \boldsymbol{E}_e} = \frac{\partial \psi_{th}}{\partial \boldsymbol{E}_e} + \frac{\partial \psi_2}{\partial \boldsymbol{E}_e}, \quad \frac{\partial \psi_m}{\partial \theta} + \frac{\partial \psi_1}{\partial \theta} = \frac{\partial \psi_{th}}{\partial \theta} + \frac{\partial \psi_2}{\partial \theta}.$$

Since ψ_1 and ψ_{th} do not depend on $\boldsymbol{E}_e$ and, similarly, ψ_2 and ψ_m do not depend on θ, it can be concluded from the previous relations that

$$\frac{\partial \psi_2}{\partial \boldsymbol{E}_e} = \frac{\partial \psi_m}{\partial \boldsymbol{E}_e}, \quad \frac{\partial \psi_1}{\partial \theta} = \frac{\partial \psi_{th}}{\partial \theta}.$$

Consequently, integrating the above expressions, one finds

$$\psi_1(\theta, \boldsymbol{\xi}) = \psi_{th}(\theta, \boldsymbol{\xi}) + \psi_3(\boldsymbol{\xi}), \quad \psi_2(\boldsymbol{E}_e, \boldsymbol{\xi}) = \psi_m(\boldsymbol{E}_e, \boldsymbol{\xi}) + \psi_3(\boldsymbol{\xi}),$$

where the function ψ_3 only depends on $\boldsymbol{\xi}$. In view of (84) or (92), ψ_3 necessarily needs to be the same in the expressions for ψ_1 and ψ_2 up to an arbitrary constant which, without loss of generality, is taken as zero. From the above relations and (84) or (92), the Helmholtz energy density can be written as

$$\hat{\psi}(\boldsymbol{E}_e, \theta, \boldsymbol{\xi}) = \psi_m(\boldsymbol{E}_e, \boldsymbol{\xi}) + \psi_{th}(\theta, \boldsymbol{\xi}) + \psi_3(\boldsymbol{\xi}). \tag{94}$$

We now turn our attention to the function $\psi_3(\boldsymbol{\xi})$ in (94) and use this function to incorporate a surface energy term as well as to satisfy additional requirements on the energy at the transformation temperature θ_T. As mentioned in Section 2, to maintain a coherent interface between stress-free austenite and stress-free twinned martensite (as well as a coherent interface between two stress-free regions of twinned martensite) a local deformation field is required, which we assume to be elastic. Fig. 7 shows schematically an austenite-twinned martensite interface at the lower and upper microscales (see also Figs. 2b and c). In the kinematic analysis of Section 2 we ignored the local elastic deformation at interfaces; hence it is not included in ψ_m given in (85). The strain energy associated to this local elastic deformation corresponds to a surface energy that can be accounted for in the model by means of the function ψ_3. Since we do not resolve the elastic deformation at the lower microscale, we propose instead a simple phenomenological formulation for the surface energy in terms of the volume fraction $\boldsymbol{\xi}$. Wang and van der Zwaag (2001) incorporated in their analysis a surface energy term based on assumptions regarding the shape and arrangement of the plates of newly formed martensite. Their model assumes that the area of the interface between austenite and twinned martensite is a *linear* function of the volume fraction $\xi^{(\alpha)}$. However, if a single transformation
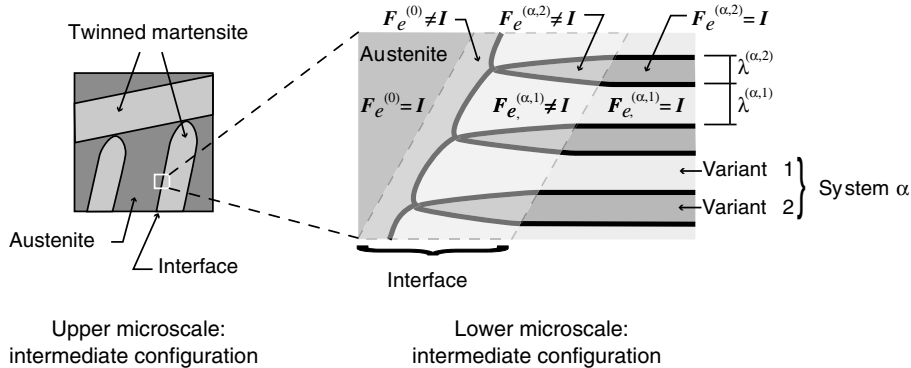

Fig. 7. Austenite-twinned martensite interface in the intermediate configuration at the lower microscale. The sketch represents an interface where the nominal stress is zero away from the interface.

system occupies a whole representative volume element at the upper microscale, this area should be zero since then there are no interfaces between austenite and martensite. This condition motivates the specific form that we propose below for the relation between the interface area and the volume fraction.

With reference to Fig. 5b and using the notation introduced in Section 2.4, let $S_x^{(\alpha)}(t)$ be the surface of a region $Y_x^{(\alpha)}(t)$ occupied by transformation system α in the reference configuration. We denote the area of the interface as $|S_x^{(\alpha)}(t)|$ and assume that

$$\frac{|S_x^{(\alpha)}(t)|}{|Y_x|} = \frac{1}{l_0} \xi^{(\alpha)}(\boldsymbol{x}, t)\left(1 - \xi^{(\alpha)}(\boldsymbol{x}, t)\right), \quad \alpha = 1, \dots, N, \tag{95}$$

where $|Y_x|$ is the volume of the RVE and the constant l_0 is a length scale parameter. If a single transformation system β occupies the whole RVE at the upper microscale, then $\xi^{(\beta)} = 1$ and $\xi^{(\alpha)} = 0$ for $\alpha = 1, \dots, N$ and $\alpha \neq \beta$. In that case, from (95), $|S_x^{(\alpha)}(t)| = 0$ for all $\alpha = 1, \dots, N$, including $\alpha = \beta$, which is consistent with the fact that there are no interfaces in the RVE. Similarly, for an RVE occupied by austenite only, $\xi^{(\alpha)} = 0$ and $|S_x^{(\alpha)}(t)| = 0$ for all $\alpha = 1, \dots, N$. Finally, we note that the surface energy at the *grain boundary* (i.e., the interface between the grain and the ferrite-based matrix) is assumed to remain the same whether the grain contains only austenite, only martensite or a mixture of both.

An interpretation of the length scale parameter l_0 can be obtained from the geometry of a plate of twinned martensite inside a grain of austenite at the *onset of transformation* (i.e., when $\xi^{(\alpha)} \ll 1$). For a small volume fraction $\xi^{(\alpha)}$, the ratio $|S_x^{(\alpha)}(t)|/|Y_x|$ can be linearized from (95) as

$$|S_x^{(\alpha)}(t)| \approx \frac{1}{l_0} |Y_x^{(\alpha)}(t)|, \quad \text{if } \xi^{(\alpha)} \ll 1,$$

where we have substituted the volume fraction by the expression given in (20). Hence, the value l_0 can be interpreted as the ratio between the initial volume and surface of twinned martensite.

Let χ be an interface energy per unit area. We assume that all austenite-twinned martensite interfaces have the same energy per unit area. Accordingly, the surface energy ψ_s per unit mass adopts the following form:

$$\psi_s(\boldsymbol{\xi}) = \frac{1}{\rho_0} \sum_{\alpha=1}^{N} \chi \frac{|S_x^{(\alpha)}(t)|}{|Y_x|} = \frac{\chi}{\rho_0 l_0} \sum_{\alpha=1}^{N} \xi^{(\alpha)}\left(1 - \xi^{(\alpha)}\right). \tag{96}$$

In (96) the summation runs over $\alpha = 1, \dots, N$; hence it does not include $\alpha = 0$ (austenite) since $\psi_s(\xi)$ corresponds to the surface energy in the austenite-twinned martensite interfaces. If $\xi^{(0)} = 0$ (i.e., RVE occupied by austenite only) but simultaneously none of the volume fractions $\xi^{(\alpha)}$ is equal to one, then it means that the RVE contains interfaces between twinned martensite with different orientations. From this point of view, the interfaces between different transformation systems (i.e., twinned martensite/twinned martensite interfaces) are assumed to have the *same* surface energy per unit area χ as the austenite/twinned martensite interfaces.

With the surface energy ψ_s as in (96), the function ψ_3 in (94) can be expressed as

$$\psi_3(\boldsymbol{\xi}) = \psi_s(\boldsymbol{\xi}) + \psi_4(\boldsymbol{\xi}),$$

where the function ψ_4 represents all energy contributions that are not included in ψ_s. From (94) and the above relation, the Helmholtz energy becomes

$$\hat{\psi}(\boldsymbol{E}_e, \theta, \boldsymbol{\xi}) = \psi_m(\boldsymbol{E}_e, \boldsymbol{\xi}) + \psi_{\text{th}}(\theta, \boldsymbol{\xi}) + \psi_s(\boldsymbol{\xi}) + \psi_4(\boldsymbol{\xi}). \tag{97}$$

As a last step in the construction of the Helmholtz energy density, the function $\psi_4(\boldsymbol{\xi})$ needs to be determined. For this purpose, we return to the definition of the transformation temperature θ_T, which is the theoretical temperature at which a stress-free austenite can transform isothermally into stress-free martensite without dissipation (or vice-versa). Since the dissipation associated with the transformation is $\mathcal{D}_{\text{tr}}$ as given

in (66), the condition for a dissipation-free transformation from austenite to system α of martensite is $f^{(\alpha)} = 0$ (since $\dot{\xi}^{(\alpha)} > 0$ during transformation). Hence, this condition requires that there is no internal energy barrier that opposes the transformation. However, in reality there are several mechanisms that contribute to an internal energy barrier. One such mechanism is the nucleation of austenite/martensite interfaces, which is taken into account in the surface energy ψ_s given in (96). Accordingly, a *theoretical* dissipation-free transformation corresponds to a vanishing surface energy (i.e., $\chi \to 0$ in (96)). Therefore, in accordance with the definition of the transformation temperature, we have

$$f^{(\alpha)}\big|_{E_e = 0, \theta = \theta_{\mathrm{T}}, \chi \to 0} = 0 \quad \forall \alpha = 1, \ldots, N \tag{98}$$

where, in view of (40), the stress-free condition $S = 0$ can be satisfied by setting $E_e = 0$. Using the expressions (73) and (97), we compute the driving force $f^{(\alpha)}$ and then use the function $\psi_4(\xi)$ to match the condition imposed in (98). To this end, we need the following derivatives: $\partial \psi_m / \partial \xi^{(\alpha)}$, $\partial \psi_{\mathrm{th}} / \partial \xi^{(\alpha)}$ and $\partial \psi_s / \partial \xi^{(\alpha)}$. From (46) and (85), the rate of change of the strain energy with respect to the volume fraction $\xi^{(\alpha)}$ is

$$\frac{\partial \psi_m}{\partial \xi^{(\alpha)}}(E_e, \xi) = \frac{1}{2\rho_0} \big((1 + \delta_{\mathrm{T}}) \mathbb{C}^{(\alpha)} - \mathbb{C}^{\mathrm{A}} \big) E_e \cdot E_e. \tag{99}$$

Similarly, from (90) and (93), the rate of change of the thermal energy with respect to the volume fraction $\xi^{(\alpha)}$ is

$$\frac{\partial \psi_{\mathrm{th}}}{\partial \xi^{(\alpha)}}(\theta, \xi) = -(h^{(\alpha)} - h^{\mathrm{A}}) \left(\theta \ln \frac{\theta}{\theta_{\mathrm{T}}} - \theta \right). \tag{100}$$

In addition, from (96), the change in surface energy is

$$\frac{\partial \psi_s}{\partial \xi^{(\alpha)}}(\xi) = \frac{\chi}{\rho_0 l_0} \big(1 - 2\xi^{(\alpha)} \big). \tag{101}$$

Combining (55), (57), (73), (78), (97), (99), (100) and (101), the driving force can be derived as

$$
\begin{aligned}
f^{(\alpha)} = {} & J_{\mathrm{tr}} F_e^{\mathrm{T}} F_e S F_{\mathrm{tr}}^{-\mathrm{T}} \cdot \gamma^{(\alpha)} + \rho_0 \theta \frac{\lambda_{\mathrm{T}}^{(\alpha)}}{\theta_{\mathrm{T}}} + \frac{1}{2} \big(\mathbb{C}^{\mathrm{A}} - (1 + \delta_{\mathrm{T}}) \mathbb{C}^{(\alpha)} \big) E_e \cdot E_e \\
& + \rho_0 (h^{(\alpha)} - h^{\mathrm{A}}) \left(\theta \ln \frac{\theta}{\theta_{\mathrm{T}}} - \theta \right) - \frac{\chi}{l_0} \big(1 - 2\xi^{(\alpha)} \big) - \rho_0 \frac{\partial \psi_4}{\partial \xi^{(\alpha)}}, \quad \alpha = 1, \ldots, N.
\end{aligned}
\tag{102}
$$

Hence, from (101) and (102), the condition (98) is satisfied if

$$f^{(\alpha)}\big|_{E_e = 0, \theta = \theta_{\mathrm{T}}, \chi \to 0} = \lambda_{\mathrm{T}}^{(\alpha)} - (h^{(\alpha)} - h^{\mathrm{A}}) \theta_{\mathrm{T}} - \frac{\partial \psi_4}{\partial \xi^{(\alpha)}} = 0, \quad \alpha = 1, \ldots, N.$$

Integrating the previous relation for each α, and using (90) for the specific heat, provides the following expression for ψ_4:

$$\psi_4(\xi) = -h(\xi) \theta_{\mathrm{T}} + \sum_{\alpha=1}^{N} \lambda_{\mathrm{T}}^{(\alpha)} \xi^{(\alpha)}, \tag{103}$$

where we have arbitrarily chosen the integration constant as zero. With the function ψ_4 chosen as in (103), from (85), (93), (96) and (97) the Helmholtz energy can be written as

$$
\begin{aligned}
\hat{\psi}(E_e, \theta, \xi) = {} & \frac{1}{2\rho_0} J_{\mathrm{tr}}(\xi) \mathbb{C}(\xi) E_e \cdot E_e - h(\xi) \theta \ln \frac{\theta}{\theta_{\mathrm{T}}} + h(\xi)(\theta - \theta_{\mathrm{T}}) - \eta_{\mathrm{T}} \theta \\
& + \sum_{\alpha=1}^{N} \lambda_{\mathrm{T}}^{(\alpha)} \xi^{(\alpha)} + \frac{\chi}{\rho_0 l_0} \sum_{\alpha=1}^{N} \xi^{(\alpha)} \big(1 - \xi^{(\alpha)} \big),
\end{aligned}
\tag{104}
$$

and, from (102) and (103), the driving force is

$$f^{(\alpha)} = f_m^{(\alpha)} + f_{\mathrm{th}}^{(\alpha)} + f_s^{(\alpha)}, \quad \alpha = 1, \ldots, N, \tag{105}$$

where the functions $f_m^{(\alpha)}$, $f_{\mathrm{th}}^{(\alpha)}$ and $f_s^{(\alpha)}$ are given by

$$f_m^{(\alpha)} := J_{\mathrm{tr}} \boldsymbol{F}_{\mathrm{e}}^{\mathrm{T}} \boldsymbol{F}_{\mathrm{e}} \boldsymbol{S} \boldsymbol{F}_{\mathrm{tr}}^{-\mathrm{T}} \cdot \boldsymbol{\gamma}^{(\alpha)} + \frac{1}{2} \left(\mathbb{C}^{\mathrm{A}} - (1 + \delta_{\mathrm{T}}) \mathbb{C}^{(\alpha)} \right) \boldsymbol{E}_{\mathrm{e}} \cdot \boldsymbol{E}_{\mathrm{e}}, \tag{106}$$

$$f_{\mathrm{th}}^{(\alpha)} := \rho_0 \frac{\lambda_{\mathrm{T}}^{(\alpha)}}{\theta_{\mathrm{T}}} (\theta - \theta_{\mathrm{T}}) + \rho_0 (h^{(\alpha)} - h^{\mathrm{A}}) \left(\theta \ln \frac{\theta}{\theta_{\mathrm{T}}} - (\theta - \theta_{\mathrm{T}}) \right), \tag{107}$$

and

$$f_s^{(\alpha)} := -\frac{\chi}{l_0} \left(1 - 2\xi^{(\alpha)} \right). \tag{108}$$

The effect of the surface energy term $f_s^{(\alpha)}$ in the driving force is as follows: If $\xi^{(\alpha)} < 0.5$, it decreases the driving force, meaning that it acts *against* transformation since it requires the formation of new interfaces. If, however, $\xi^{(\alpha)} > 0.5$, this term acts *in favor* of the transformation. The interpretation of the latter phenomenon is that *one* transformation system is in the process of occupying the whole grain and, as a result, martensitic plates of that system are coalescing (thus interfaces disappear and the surface energy is "released").

5.2. Onset of transformation and kinetic relation

In order to describe the onset and evolution of phase transformations, a nucleation criterion and a kinetic law need to be specified (Abeyaratne and Knowles, 1991). The onset of a transformation from austenite to a system α of martensite occurs when the energy available for the transformation is equal to an internal energy barrier. As mentioned in Section 5.1, the internal energy barrier consists of various contributions, among which the nucleation of new interfaces is explicitly taken into account through the surface energy term $f_s^{(\alpha)}$. The remaining contributions, which are not explicitly quantified, are collected in a critical threshold value $f_{\mathrm{cr}}^{(\alpha)}$ for the driving force. Therefore, the criterion for the initiation of a martensitic phase transformation is

$$f^{(\alpha)} = f_{\mathrm{cr}}^{(\alpha)} \quad \text{(onset of transformation)}.$$

When transformation is activated, the growth rate $\dot{\xi}^{(\alpha)}$ of a transformation system α is supposed to depend on the amount by which the driving force exceeds the threshold level (i.e., $f^{(\alpha)} - f_{\mathrm{cr}}^{(\alpha)}$). From a crystallographic point of view, martensitic transformations in shape memory alloys are reversible in the sense that martensite transforms back to austenite upon unloading. In contrast, reverse transformations of martensite upon unloading are typically not observed in multiphase carbon steels. In the examples shown in Section 6 we will apply the model to crystallographically irreversible transformations. Since the model developed here does not prevent reversible transformations, it needs to be specialized to take the irreversibility upon unloading into account. One method is to introduce a sufficiently large absolute value for the critical driving force required for a martensite to austenite transformation. An alternative method, simpler to implement, is to introduce the following phenomenological kinetic relation for the evolution of the transformation:

$$\dot{\xi}^{(\alpha)} = \dot{\xi}_{\max}^{(\alpha)} \tanh \left(\frac{1}{\nu^{(\alpha)}} \frac{\langle f^{(\alpha)} - f_{\mathrm{cr}}^{(\alpha)} \rangle}{f_{\mathrm{cr}}^{(\alpha)}} \right), \tag{109}$$

where the Macauley brackets are such that $\langle g \rangle = g$ if $g \geq 0$ and equal to zero otherwise. Further, $v^{(\alpha)} > 0$, $f_{cr}^{(\alpha)} > 0$ and $\dot{\xi}_{max}^{(\alpha)} \geq 0$ are material parameters. We interpret $v^{(\alpha)}$ as a dimensionless, viscosity-like parameter and $\dot{\xi}_{max}^{(\alpha)}$ as maximum value for the transformation rate. In view of (109), if $f^{(\alpha)} < f_{cr}^{(\alpha)}$ then $\dot{\xi}^{(\alpha)} = 0$. Moreover, the rates $\dot{\xi}^{(\alpha)}$ are restricted to non-negative values. Consequently, the martensite cannot transform back into austenite. Note that the kinetic relation (109) is *consistent* with the isothermal dissipation inequality (66) for *any* value of $f^{(\alpha)}$. Applications of this model for irreversible transformations in carbon steels can be found in Turteltaub and Suiker (2005) and Suiker and Turteltaub (2005).

5.3. Heat conduction and latent heat

To complete the thermal aspects of the model, a relation between the entropy flux $\mathbf{\Phi}$ and its corresponding affinity, the temperature gradient $\nabla\theta$, is required. This relation is formally similar to a kinetic relation. The most commonly used constitutive relation to describe this effect is Fourier's model $\boldsymbol{q} = -\boldsymbol{K}\nabla\theta$, where $\boldsymbol{K}$ is the thermal conductivity tensor. From (47) and Fourier's model, the relation between the entropy flux and the temperature gradient becomes

$$\mathbf{\Phi} = -\frac{\boldsymbol{K}}{\theta}\nabla\theta. \tag{110}$$

From (65), the dissipation inequality in the absence of a phase change becomes $\mathscr{D}_q \geq 0$ and, in view of (62), is satisfied if $\boldsymbol{K}$ is positive semi-definite.

In order to relate the thermal parameters of the model to experimental data, it is useful to develop an explicit expression for the latent heat for isothermal transformations. Let $\lambda^{(\alpha)}(\theta)$ denote the latent heat for a complete transformation from pure austenite ($\xi^{(0)} = 1$, $\xi^{(\alpha)} = 0$) to a single system α of martensite ($\xi^{(0)} = 0$, $\xi^{(\alpha)} = 1$) at a temperature θ. By definition, $\lambda^{(\alpha)}(\theta)$ is given by

$$\lambda^{(\alpha)}(\theta) := \theta\Delta\eta^{(\alpha)},$$

where $\Delta\eta^{(\alpha)}$ represents the total change in entropy during the transformation. From (48), (49), (89) and (90), we have

$$\lambda^{(\alpha)}(\theta) = \theta\left[(\eta_e + \eta_{tr})|_{\xi^{(\alpha)}=1} - (\eta_e + \eta_{tr})|_{\xi^{(\alpha)}=0}\right] = (h^{(\alpha)} - h^A)\theta\ln\frac{\theta}{\theta_T} + \theta\frac{\lambda_T^{(\alpha)}}{\theta_T}. \tag{111}$$

Knowledge of the specific heats and the latent heat at some temperature θ can be used to compute the latent heat $\lambda_T^{(\alpha)}$ at the theoretical transformation temperature θ_T using expression (111). We remark that, from the thermal point of view, the existence of an energy barrier implies that a transformation at zero stress from austenite to martensite does not occur at the theoretical transformation temperature θ_T; rather, this occurs at a lower temperature, usually denoted as M_s. Accordingly, from (111), we obtain

$$\lambda_T^{(\alpha)} = \frac{\theta_T}{M_s}\left(\lambda^{(\alpha)}(M_s) - (h^{(\alpha)} - h^A)M_s\ln\frac{M_s}{\theta_T}\right).$$

5.4. Summary of main model equations

For convenience, we summarize below the main ingredients of the model and we point out the duality between the mechanical and thermal parts. The decompositions of the primary variables (i.e., deformation gradient (12) and entropy (48)) are

$$\boldsymbol{F} = \boldsymbol{F}_e\boldsymbol{F}_{tr}, \quad \eta = \eta_e + \eta_{tr}.$$

The expressions for the transformation parts in the above relations (i.e., the transformation deformation gradient from (24) and the transformation entropy (49)) are

$$\boldsymbol{F}_{\text{tr}} = \boldsymbol{I} + \sum_{\alpha=1}^{N} \xi^{(\alpha)} \boldsymbol{\gamma}^{(\alpha)}, \quad \eta_{\text{tr}} = \sum_{\alpha=1}^{N} \xi^{(\alpha)} \frac{\lambda_{\text{T}}^{(\alpha)}}{\theta_{\text{T}}}.$$

The constitutive relations between conjugate variables (i.e., stress and elastic strain from (40) and temperature and reversible entropy from (89)) are

$$\boldsymbol{S} = \mathbb{C}\boldsymbol{E}_{\text{e}}, \quad \eta_{\text{e}} = h \ln \frac{\theta}{\theta_{\text{T}}} + \eta_{\text{T}}.$$

The effective stiffness and the effective specific heat (from (46) and (90)) are

$$\mathbb{C} = \frac{1}{J_{\text{tr}}} \left\{ \left(1 - \sum_{\alpha=1}^{N} \xi^{(\alpha)} \right) \mathbb{C}^{\text{A}} + (1 + \delta_{\text{T}}) \sum_{\alpha=1}^{N} \xi^{(\alpha)} \mathbb{C}^{(\alpha)} \right\},$$

$$h = \left(1 - \sum_{\alpha=1}^{N} \xi^{(\alpha)} \right) h^{\text{A}} + \sum_{\alpha=1}^{N} \xi^{(\alpha)} h^{(\alpha)}.$$

The relation between the affinities and the fluxes (for the transformation from (109) and for heat conduction from (110)) are given by

$$\dot{\xi}^{(\alpha)} = \dot{\xi}_{\text{max}}^{(\alpha)} \tanh \left(\frac{1}{\nu^{(\alpha)}} \frac{\langle f^{(\alpha)} - f_{\text{cr}}^{(\alpha)} \rangle}{f_{\text{cr}}^{(\alpha)}} \right),$$

$$\boldsymbol{\Phi} = -\frac{\boldsymbol{K}}{\theta} \nabla \theta,$$

where the driving force for the transformation is, from (105)–(108)

$$f^{(\alpha)} = J_{\text{tr}} \boldsymbol{F}_{\text{e}}^{\text{T}} \boldsymbol{F}_{\text{e}} \boldsymbol{S} \boldsymbol{F}_{\text{tr}}^{-\text{T}} \cdot \boldsymbol{\gamma}^{(\alpha)} + \frac{1}{2} \left(\mathbb{C}^{\text{A}} - (1 + \delta_{\text{T}}) \mathbb{C}^{(\alpha)} \right) \boldsymbol{E}_{\text{e}} \cdot \boldsymbol{E}_{\text{e}}$$

$$+ \rho_0 \frac{\lambda_{\text{T}}^{(\alpha)}}{\theta_{\text{T}}} (\theta - \theta_{\text{T}}) + \rho_0 (h^{(\alpha)} - h^{\text{A}}) \left(\theta \ln \frac{\theta}{\theta_{\text{T}}} - (\theta - \theta_{\text{T}}) \right) - \frac{\chi}{l_0} \left(1 - 2\xi^{(\alpha)} \right).$$

The above equations are in correspondence with a Helmholtz energy given by (104), i.e.,

$$\hat{\psi}(\boldsymbol{E}_{\text{e}}, \theta, \boldsymbol{\xi}) = \frac{1}{2\rho_0} J_{\text{tr}}(\boldsymbol{\xi}) \mathbb{C}(\boldsymbol{\xi}) \boldsymbol{E}_{\text{e}} \cdot \boldsymbol{E}_{\text{e}} - h(\boldsymbol{\xi}) \theta \ln \frac{\theta}{\theta_{\text{T}}} + h(\boldsymbol{\xi})(\theta - \theta_{\text{T}}) - \eta_{\text{T}} \theta$$

$$+ \sum_{\alpha=1}^{N} \lambda_{\text{T}}^{(\alpha)} \xi^{(\alpha)} + \frac{\chi}{\rho_0 l_0} \sum_{\alpha=1}^{N} \xi^{(\alpha)} \left(1 - \xi^{(\alpha)} \right).$$

6. Single-crystal deformations

To illustrate the basic features of the model, several simple deformations of a cubic domain Ω are analyzed in this section. More complex boundary value problems, involving transforming grains of austenite embedded in a ferritic matrix, are presented elsewhere (Turteltaub and Suiker, 2005; Suiker and Turteltaub, 2005). In the present examples, for simplicity, only isothermal processes are considered (at $\theta = 300$ K). The domain Ω consists initially of an undeformed single crystal of austenite. As a global coordinate system we use an orthonormal vector basis $\{\boldsymbol{f}_1, \boldsymbol{f}_2, \boldsymbol{f}_3\}$ with the basis vectors pointing in directions

normal to three mutually perpendicular faces of the domain Ω. For a single-crystal of austenite the lattice orientation is given in terms of basis vectors $\{e_1^A, e_2^A, e_3^A\}$ aligned with the cubic lattice axes. We study the mechanical response of the material for two representative orientations of the crystal lattice under various loading conditions. The two crystal orientations are specified as follows:

Orientation 1 ($[1\,1\,1]_A$):

$$\boldsymbol{f}_1 = \frac{1}{\sqrt{3}}\left(\boldsymbol{e}_1^A + \boldsymbol{e}_2^A + \boldsymbol{e}_3^A\right), \quad \boldsymbol{f}_2 = \frac{1}{\sqrt{2}}\left(\boldsymbol{e}_1^A - \boldsymbol{e}_3^A\right), \quad \boldsymbol{f}_3 = \frac{1}{\sqrt{6}}\left(-\boldsymbol{e}_1^A + 2\boldsymbol{e}_2^A - \boldsymbol{e}_3^A\right).$$

Orientation 2 ($[1\,0\,0]_A$):

$$\boldsymbol{f}_k = \boldsymbol{e}_k^A, \quad k = 1, 2, 3.$$

Orientations 1 and 2 are henceforth referred to as $[1\,1\,1]_A$ and $[1\,0\,0]_A$, respectively. The subindex 'A' indicates that the components of the global vector $\boldsymbol{f}_1$ are expressed in the austenite lattice basis. The mechanical properties used in the isothermal simulations, which correspond to the austenitic and martensitic phases in a multiphase carbon steel with a local carbon concentration of 1.4 wt.%, are listed in Table 1. The characteristics of the transformation systems are presented in Appendix A (Table A.1). Details on the derivation of the properties and the computation of the effective stiffness tensors $\mathbb{C}^{(\alpha)}$ can be found in Turteltaub and Suiker (2005). Details of the numerical implementation of the transformation model can be found in Suiker and Turteltaub (2005).

6.1. Uniaxial deformations

For each crystal orientation, a uniaxial extension followed by a uniaxial compression is prescribed. The specific boundary conditions are as follows: on three mutually perpendicular faces of the cubic domain, the displacement *normal* to each face is set to zero. On one of the faces perpendicular to the global direction $\boldsymbol{f}_1$ (opposite to the constrained face) the normal displacement is set to

$$u_1 = \hat{u}_1(t) = \begin{cases} 10^{-4} l t & \text{for } 0 \leqslant t \leqslant T/2, \\ -10^{-4} l (t - T) & \text{for } T/2 \leqslant t \leqslant T, \end{cases} \tag{112}$$

where l is the side length of the cubic domain and T is the total duration of the deformation process. In (112) the nominal strain rate for extension and compression is given as 10^{-4} s^{-1}, measured in terms of the relative velocities of the two opposite external surfaces that are perpendicular to the $\boldsymbol{f}_1$-direction. The tangential stresses on the constrained faces are zero and the unconstrained faces are stress-free. The total duration of the deformation process is $T = 300$ s and $T = 1200$ s for the $[1\,1\,1]_A$ and $[1\,0\,0]_A$ crystal orientations, respectively. The duration T in each case is chosen such that at $t = T/2$ approximately 50% of the austenite has transformed into martensite.

The orientations and boundary conditions are shown in Fig. 8. The mechanical response of the material is reported in terms of the Cauchy stress $\boldsymbol{T}$ and the logarithmic strain $\boldsymbol{e}$. The logarithmic strain is defined as

Table 1
Material properties for the transformation model based on austenite and martensite in a multiphase carbon steel

Austenite	$\kappa_1^A = 268.5$, $\kappa_2^A = 156$, $\kappa_3^A = 136$ [GPa]
Martensite	$\kappa_1^M = 497$, $\kappa_2^M = 405$, $\kappa_3^M = 265$, $\kappa_4^M = 617$, $\kappa_5^M = 263$, $\kappa_6^M = 287$ [GPa]
Transformation strain and dilation	$\gamma_T = 0.1809$, $\delta_T = 0.0391$
Transformation kinetics	$\nu = 0.17$, $\dot{\xi}_{\max} = 3 \times 10^{-3}$ s^{-1}
Critical transformation value	$f_{cr}^{(\alpha)} - f_{th}(\theta) = 5$ MPa at $\theta = 300$ K
Surface energy	$\chi = 0.2$ J m^{-2}, $l_0 = 0.05$ μm.

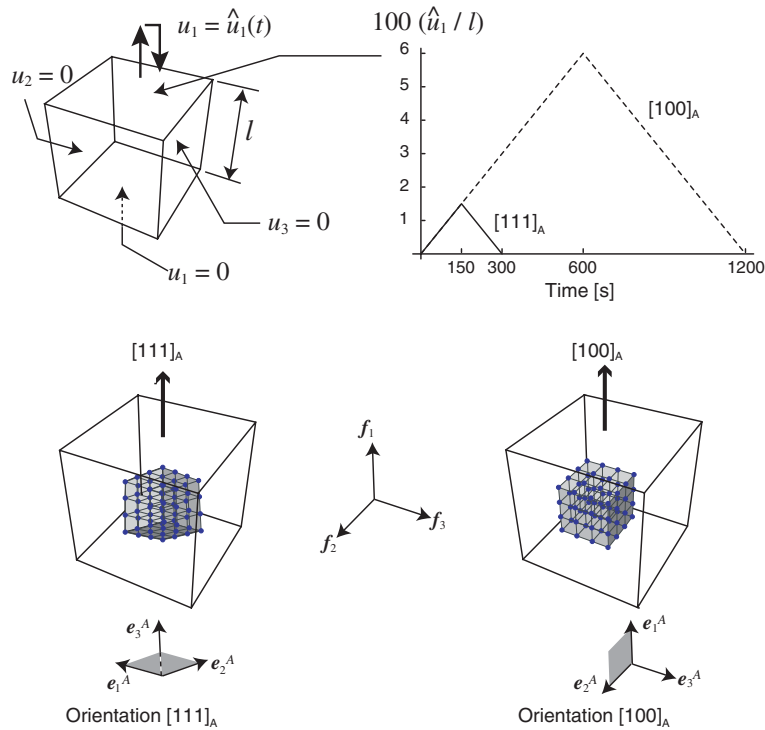Fig. 8. Crystal orientations and boundary conditions for uniaxial extension followed by uniaxial compression.

$e := \ln V$, where V is the left stretch tensor in the polar decomposition of the total deformation gradient F, i.e., $V = FR^T$, with R corresponding to the rigid body rotation. The component T_{11} of the Cauchy stress (referred to the global basis) as a function of the component e_{11} of the logarithmic strain is shown in Fig. 9a for orientations $[1\,1\,1]_A$ (curve 1) and $[1\,0\,0]_A$ (curve 2). For comparison, the response of the material to *monotonic extension* is also shown for crystal orientations $[1\,1\,1]_A$ (curve 3) and $[1\,0\,0]_A$ (curve 4).

The stress-strain curves for extension followed by compression consist of several stages. During the extension part, the deformation is initially elastic until the austenite starts to transform into martensite. During transformation, the stress-strain response shows a plateau, which indicates that the material parameters for the kinetic law in combination with the applied strain rate provide a behavior close to a rate-independent response (Anand and Gurtin, 2003). Upon reversal of the displacement from extension to compression, the transformation systems that were active cease to transform and the deformation becomes elastic. Subsequently, the transformation resumes in compression with other transformation systems being activated. For the $[1\,0\,0]_A$ orientation (curve 2), the material fully transforms into martensite and subsequently behaves elastically. In contrast, for the $[1\,1\,1]_A$ orientation (curve 1) the transformation is far from complete at the end of the compressive part.

The specific transformation systems that are active during deformation are shown in Fig. 9b for orientations $[1\,1\,1]_A$ and $[1\,0\,0]_A$ (curves 1 and 2, respectively). Observe that the transformation from austenite to martensite is irreversible; hence the martensite formed during extension remains in the microstructure during compression. Moreover, for orientation $[1\,0\,0]_A$ the transformation in compression starts soon after the displacement is reversed whereas for orientation $[1\,1\,1]_A$ a considerable stress build-up in compression is required before the transformation becomes once again active. These results are in agreement with simulations of uniaxial monotonic extension and monotonic compression presented in Turteltaub and Suiker
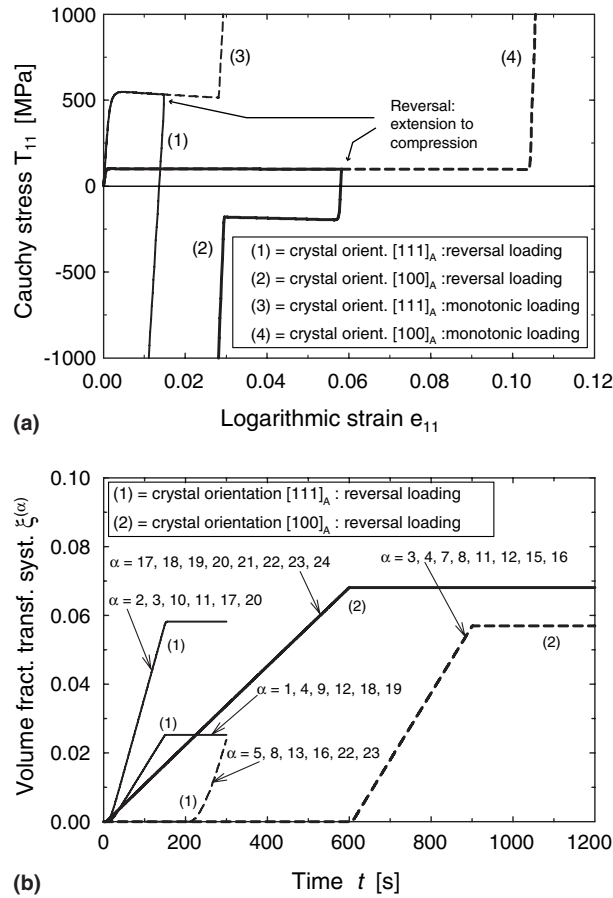
Fig. 9. (a) Axial Cauchy stress component T_{11} vs. axial logarithmic strain e_{11} for crystal orientations $[1\,1\,1]_A$ (curve 1) and $[1\,0\,0]_A$ (curve 2) under extension followed by compression. Curves (3) and (4) correspond to monotonically increasing uniaxial extension for orientations $[1\,1\,1]_A$ and $[1\,0\,0]_A$ respectively; (b) Martensite volume fractions $\xi^{(\alpha)}$ of transformation systems α as a function of time for crystal orientations $[1\,1\,1]_A$ (curves 1) and $[1\,0\,0]_A$ (curves 2) under extension followed by compression. Solid lines represent transformation systems active during extension while dashed lines correspond to transformation systems active during compression.

(2005), where it was observed that austenite in the $[1\,0\,0]_A$ orientation offers less resistance to transformation than austenite in the $[1\,1\,1]_A$ orientation. The simulation results are also in agreement with experimental observations of Oliver et al. (2002) and Kruijver et al. (2003), which demonstrate that the $[1\,1\,1]_A$ and $[1\,0\,0]_A$ are, respectively, "strong" and "weak" directions of the transforming austenitic grain.

6.2. Simple shear

For simple shear, the deformation $\hat{y}$ referred to the global basis $\{f_i\}$ is given by $\hat{y}_1(x) = x_1 + \gamma x_2$, $\hat{y}_2(x) = x_2$ and $\hat{y}_3(x) = x_3$, where γ is the amount of shear. As in the previous subsection, the response of a single-crystal of austenite is analyzed for the $[1\,1\,1]_A$ and $[1\,0\,0]_A$ orientations. The amount of shear is applied at a rate $\dot{\gamma} = 10^{-4}$ s^{-1}. The crystal orientations and boundary conditions for simple shear are shown in Fig. 10. The components T_{ij} of the Cauchy stress tensor (referred to the global basis) as functions of the amount of shear γ are shown in Figs. 11a and 12a for orientations $[1\,1\,1]_A$ and $[1\,0\,0]_A$, respectively. The
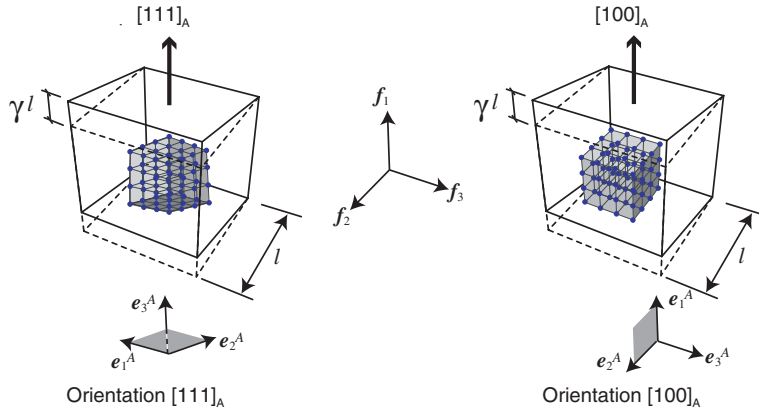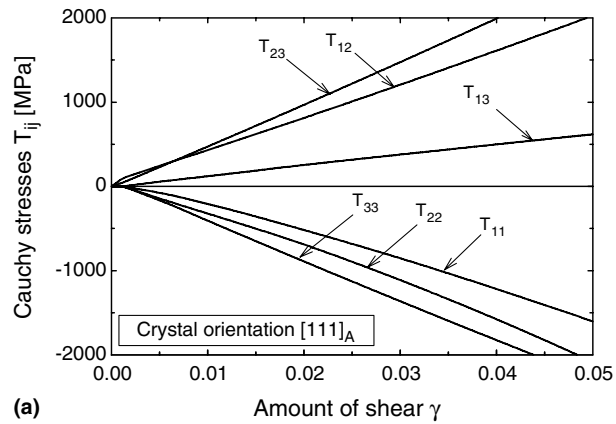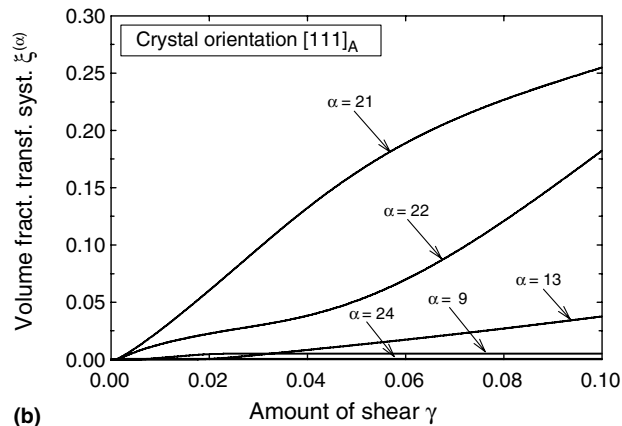
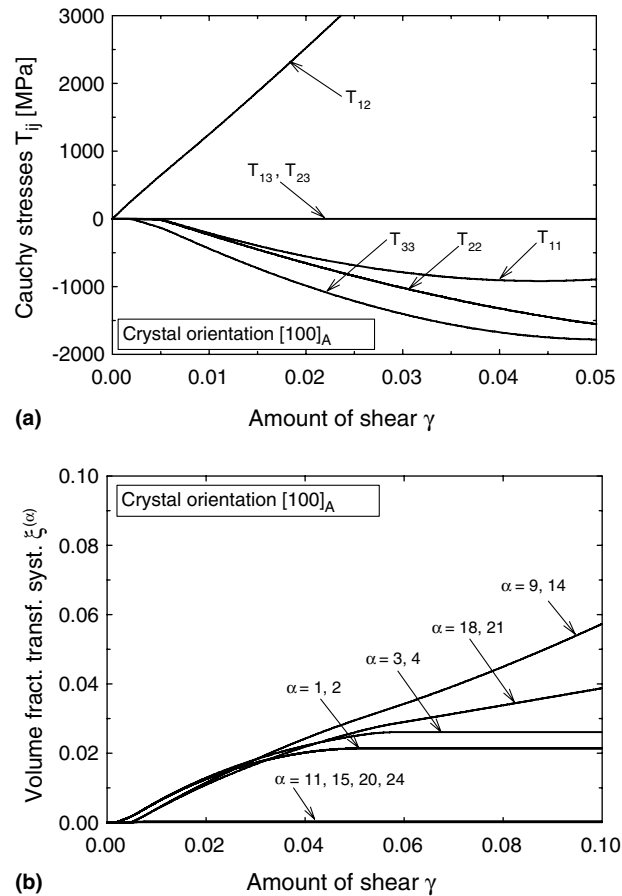Fig. 10. Crystal orientations for simple shear.

Fig. 11. Crystal orientation $[1\,1\,1]_A$: (a) Cauchy stress components T_{ij} vs. amount of shear γ for simple shear; (b) Martensite volume fractions $\xi^{(\alpha)}$ of transformation systems α vs. amount of shear γ.

Fig. 12. Crystal orientation $[1\,0\,0]_A$: (a) Cauchy stress components T_{ij} vs. amount of shear γ for simple shear; (b) Martensite volume fractions $\xi^{(\alpha)}$ of transformation systems α vs. amount of shear γ.

corresponding evolutions of active transformation systems as a function of the amount of shear are presented in Figs. 11b and 12b.

Under simple shear, the directions of the principal stresses evolve during the loading process. As shown in Figs. 11b and 12b, this relates to a gradual change in activity of the transformation systems. Fig. 12a illustrates that for the $[1\,0\,0]_A$ orientation the highest stress component corresponds to T_{12}. In contrast, for the $[1\,1\,1]_A$ orientation, the T_{12} component of the stress, which initially is the largest, is overtaken by the T_{23} component as the amount of shear increases (see Fig. 11a). Furthermore, the T_{11}, T_{22} and T_{33} components substantially contribute to the stress state.

6.3. Volumetric expansion and contraction

For volumetric expansion and contraction, the deformation $\hat{y}$ referred to the global basis $\{f_i\}$ is given by $\hat{y}_i(x) = \lambda x_i$, $i = 1, 2, 3$, with $\lambda > 1$ for expansion and $\lambda < 1$ for contraction. The Jacobian of this deformation
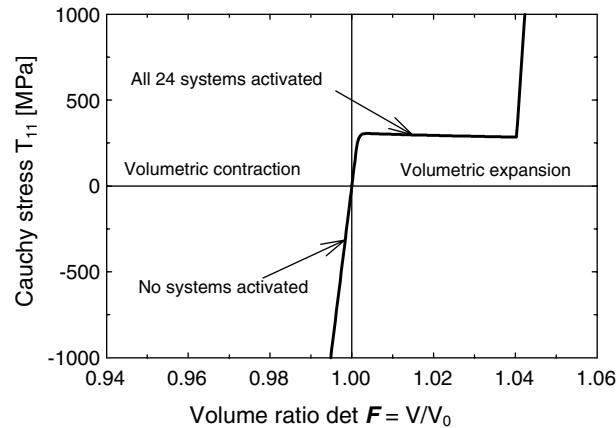
Fig. 13. Cauchy stress component T_{11} ($=T_{22} = T_{33}$) vs. volume ratio $J = \det F$ for all crystal orientations under volumetric contraction ($J < 1$) and expansion ($J > 1$).

is $J = \det F = \lambda^3 = V/V_0$, where V is the volume of the domain in the current configuration and V_0 is the volume in the reference configuration. The deformation rate is taken as $\dot{\lambda} = 10^{-4}$ s^{-1}. For all crystal orientations, the Cauchy stress component T_{11} ($= T_{22} = T_{33}$) as a function of the volume ratio $J = V/V_0$ is shown in Fig. 13. The stress components T_{12}, T_{23} and T_{23} are zero throughout the deformation. During volumetric expansion, the response is initially elastic followed by a transformation part that is characterized by a plateau-like response. All transformation systems are equally active during the transformation, i.e., $\xi^{(\alpha)} = \xi$ for $\alpha = 1, \dots, N$. After the austenite has fully transformed into martensite, the deformation proceeds elastically. In contrast, during volumetric contraction, no transformation systems are activated and the deformation is elastic in the austenitic phase. The difference in behavior between volumetric expansion and contraction is due to the fact that the phase change from austenite to martensite is accompanied by a dilatational change (equal to δ_T as given in (44)), which is prevented during volumetric contraction.

7. Concluding remarks

The multiscale thermomechanical model for cubic to tetragonal martensitic phase transformations presented in this paper incorporates effects associated to microstructural information from several subgrain length scales. In particular, the crystallographic orientations of individual layers of tetragonal martenstic variants are preserved in the mesoscale stiffness tensor. This information is accounted for explicitly in the expression for the transformation driving force. Consequently, the so-called "variant selection criterion" is improved in comparison to other martensitic transformation models. More specifically, the characteristics of each transformation system enter the selection criterion not only through the orientation of the habit plane (via the tensor $\gamma^{(\alpha)}$ in the expression of the driving force $f^{(\alpha)}$) but also through the *internal structure* of the twinned martensite (via the constitutive tensor $\mathbb{C}^{(\alpha)}$ that appears in $f^{(\alpha)}$).

The model predicts a "plateau" type stress–strain response under uniaxial and volumetric deformations, which is typically observed in martensitic phase transformations under quasi-static loading (Miyazaki, 1996). During transformation, the model *automatically* selects the energetically most favorable combination of transformation systems, which depends on the externally-imposed deformation. Furthermore, as shown in Section 6.1, the model can handle non-monotonic loadings in a robust fashion. The present paper

presents the theoretical framework of the transformation model, and validations of the model based on comparisons with experimental data on multiphase carbon steels can be found in Turteltaub and Suiker (2005) and Suiker and Turteltaub (2005).

Although we have focussed attention to cubic to tetragonal transformations, the model can be readily adapted to simulate austenite to twinned α'-martensite transformations for non-tetragonal variants of martensite. This can be achieved by modifying the number and the geometrical characteristics of the transformation systems.

Acknowledgements

Appendix A. Transformation systems

See Table A.1.

Table A.1
Geometrical characteristics of the transformation systems α of martensite (referred to the lattice basis of austenite and based on a carbon concentration of 1.4 wt.%): the tetragonal variants β_1 and β_2 are layered in volumetric proportions $\lambda^{(\alpha,\beta_1)}$ and $\lambda^{(\alpha,\beta_2)} = 1 - \lambda^{(\alpha,\beta_1)}$

α	(β_1, β_2)	$\lambda^{(\alpha,\beta_1)}$	Normalized shape strain: $[\hat{\boldsymbol{b}}^{(\alpha)}]_A$	Habit plane normal: $[\boldsymbol{m}^{(\alpha)}]_A$
1	(1, 2)	0.3998	[−0.1906, 0.6311, −0.7520]	[0.1711, −0.5666, −0.8060]
2	(1, 2)	0.3998	[0.1906, −0.6311, −0.7520]	[−0.1711, 0.5666, −0.8060]
3	(1, 2)	0.6002	[−0.6311, 0.1906, −0.7520]	[0.5666, −0.1711, −0.8060]
4	(1, 2)	0.6002	[0.6311, −0.1906, −0.7520]	[−0.5666, 0.1711, −0.8060]
5	(1, 2)	0.3998	[0.1906, 0.6311, −0.7520]	[−0.1711, −0.5666, −0.8060]
6	(1, 2)	0.3998	[−0.1906, −0.6311, −0.7520]	[0.1711, 0.5666, −0.8060]
7	(1, 2)	0.6002	[−0.6311, −0.1906, −0.7520]	[0.5666, 0.1711, −0.8060]
8	(1, 2)	0.6002	[0.6311, 0.1906, −0.7520]	[−0.5666, −0.1711, −0.8060]
9	(1, 3)	0.3998	[−0.1906, −0.7520, 0.6311]	[0.1711, −0.8060, −0.5666]
10	(1, 3)	0.3998	[0.1906, −0.7520, −0.6311]	[−0.1711, −0.8060, 0.5666]
11	(1, 3)	0.6002	[−0.6311, −0.7520, 0.1906]	[0.5666, −0.8060, −0.1711]
12	(1, 3)	0.6002	[0.6311, −0.7520, −0.1906]	[−0.5666, −0.8060, 0.1711]
13	(1, 3)	0.3998	[0.1906, −0.7520, 0.6311]	[−0.1711, −0.8060, −0.5666]
14	(1, 3)	0.3998	[−0.1906, −0.7520, −0.6311]	[0.1711, −0.8060, 0.5666]
15	(1, 3)	0.6002	[−0.6311, −0.7520, −0.1906]	[0.5666, −0.8060, 0.1711]
16	(1, 3)	0.6002	[0.6311, −0.7520, 0.1906]	[−0.5666, −0.8060, −0.1711]
17	(2, 3)	0.3998	[−0.7520, 0.1906, −0.6311]	[−0.8060, −0.1711, 0.5666]
18	(2, 3)	0.3998	[−0.7520, −0.1906, 0.6311]	[−0.8060, 0.1711, −0.5666]
19	(2, 3)	0.6002	[−0.7520, 0.6311, −0.1906]	[−0.8060, −0.5666, 0.1711]
20	(2, 3)	0.6002	[−0.7520, −0.6311, 0.1906]	[−0.8060, 0.5666, −0.1711]
21	(2, 3)	0.3998	[−0.7520, −0.1906, −0.6311]	[−0.8060, 0.1711, 0.5666]
22	(2, 3)	0.3998	[−0.7520, 0.1906, 0.6311]	[−0.8060, −0.1711, −0.5666]
23	(2, 3)	0.6002	[−0.7520, 0.6311, 0.1906]	[−0.8060, −0.5666, −0.1711]
24	(2, 3)	0.6002	[−0.7520, −0.6311, −0.1906]	[−0.8060, 0.5666, 0.1711]

References

Abeyaratne, R., Knowles, J.K., 1990. On the driving traction acting on a surface of strain discontinuity in a continuum. J. Mech. Phys. Solids 38 (3), 345–360.

Abeyaratne, R., Knowles, J.K., 1991. Kinetic relations and the propagation of phase boundaries in solids. Arch. Ration. Mech. Anal. 114 (2), 119–154.

Anand, L., Gurtin, M.E., 2003. Thermal effects in the superelasticity of crystalline shape-memory materials. J. Mech. Phys. Solids 51 (6), 1015–1058.

Ball, J.M., James, R.D., 1987. Fine phase mixtures as minimizers of energy. Arch. Ration. Mech. Anal. 100 (1), 13–52.

Bhattacharya, K., 1993. Comparison of the geometrically nonlinear and linear theories of martensitic-transformation. Continuum Mech. Therm. 5 (3), 205–242.

Bhattacharya, K., 1999. Phase boundary propagation in a heterogeneous body. Proc. R. Soc. Lond. A 455, 757–766.

Bhattacharyya, A., Weng, G.J., 1994. An energy criterion for stress-induced martensitic transformation in a ductile system. J. Mech. Phys. Solids 42 (11), 1699–1724.

Callen, H.B., 1985. Thermodynamics and an Introduction to Thermostatistics, 2nd ed. John Wiley & Sons.

Christian, J.W., 2002. The Theory of Transformations in Metals and Alloys (Part II), third ed. Pergamon Press.

Coleman, B.D., Noll, W., 1963. The thermodynamics of elastic materials with heat conduction and viscosity. Arch. Ration. Mech. Anal. 13 (3), 167–178.

Diani, J.M., Parks, D.M., 1998. Effects of strain state on the kinetics of strain-induced martensite in steels. J. Mech. Phys. Solids 46 (9), 1613–1635.

Fischer, F.D., Oberaigner, E.R., Tanaka, K., Nishimura, F., 1998. Transformation induced plasticity revised an updated formulation. Int. J. Solids Struct. 35 (18), 2209–2227.

Govindjee, S., Miehe, C., 2001. A multi-variant martensitic phase transformation model: formulation and numerical implementation. Comput. Method. Appl. Mech. Eng. 191, 215–238.

Hane, K.F., Shield, T.W., 1998. Symmetry and microstructure in martensites. Phil. Mag. A 78 (6), 1215–1252.

Hane, K.F., Shield, T.W., 1999. Microstructure in the cubic to monoclinic transition in titanium-nickel shape memory alloys. Acta Mater. 47 (9), 2603–2617.

Havner, K.S., 1973. Mechanics of crystalline solids. J. Mech. Phys. Solids 21 (6), 383–394.

Huang, M., Brinson, L.C., 1999. A multivariant model for single crystal shape memory alloy behavior. J. Mech. Phys. Solids 46, 1379–1409.

Hill, R., Rice, J.R., 1972. Constitutive analysis of elastic–plastic crystals at arbitrary strain. J. Mech. Phys. Solids 20 (6), 401–413.

Idesman, A.V., Levitas, V.I., Stein, E., 1999. Elastoplastic materials with martensitic phase transition and twinning at finite strains: numerical solution with the finite element method. Comput. Method. Appl. Mech. Eng. 173, 71–98.

James, R.D., Hane, K.F., 2000. Martensitic transformations and shape-memory materials. Acta Mater. 48 (1), 197–222.

Jannetti, C., Bassani, J.L., Turteltaub, S., 2004. Thermodynamic driving forces for martensitic phase transformations in shape-memory alloys. In: Mater. Res. Soc. Symp. Proc., 855E, W5.2.

Kruijver, S.O., Zhao, L., Sietsma, J., Offerman, S.E., van Dijk, N.H., Lauridsen, E.M., Margulies, L., Grigull, S., Poulsen, H.F., van der Zwaag, S., 2003. In situ observations on the mechanical stability of austenite in TRIP-steel. J. Phys. IV 104, 499–502.

Leblond, J.B., Mottet, G., Devaux, J.C., 1986a. A theoretical and numerical approach to the plastic behavior of steels during phase-transformations—I. Derivation of general relations. J. Mech. Phys. Solids 34 (4), 395–409.

Leblond, J.B., Mottet, G., Devaux, J.C., 1986b. A theoretical and numerical approach to the plastic behaviour of steels during phase transformations—I. Study of classical plasticity for ideal-plastic phases. J. Mech. Phys. Solids 34 (4), 411–432.

Lee, E.H., 1969. Elastic–plastic deformation at finite strains. J. Appl. Mech. 36 (1), 1–6.

Levitas, V.I., Idesman, A.V., Stein, E., 1999. Shape memory alloys: micromechanical modeling and numerical analysis of structures. J. Intel. Mater. Syst. Struct. 10, 983–996.

Liu, I-S., 2002. Continuum Mechanics. Springer, Berlin.

Marketz, F., Fischer, F.D., 1994. Micromechanical modelling of stress-assisted martensitic transformation. Modell. Simul. Mater. Sci. Eng. 2, 1017–1046.

Marketz, F., Fischer, F.D., 1995. A mesoscale study on the thermodynamic effect of stress on martensitic transformation. Metall. Mater. Trans. A 26, 267–278.

Miyazaki, S., 1996. Development and characterization of shape memory alloys. In: Shape Memory Alloys, International Centre for Mechanical Sciences, Number 351, Springer, Vienna, New York, pp. 69–147.

Oliver, E.C., Withers, P.J., Daymond, M.R., Ueta, S., Mori, T., 2002. Neutron-diffraction study of stress-induced martensitic transformation in TRIP steel. Appl. Phys. A 74, S1143–S1145.

Olson, G.B., Cohen, M., 1975. Kinetics of strain-induced martensitic nucleation. Metall. Trans. A 6 (4), 791–795.

Rao, B.V.N., Rashid, M.S., 1997. Direct observations of deformation-induced retained austenite transformation in a vanadium-containing dual-phase steel. Mater. Charact. 39 (2–5), 435–453.

Rice, J.R., 1971. Inelastic constitutive relations for solids—an internal-variable theory and its application to metal plasticity. J. Mech. Phys. Solids 19 (6), 433–455.

Simo, J.C., Miehe, C., 1992. Associative coupled thermoplasticity at finite strains—formulation, numerical-analysis and implementation. Comput. Method. Appl. Mech. Eng. 98 (1), 41–104.

Stringfellow, R.G., Parks, D.M., Olson, G.B., 1992. A constitutive model for transformation plasticity accompanying strain-induced martensitic transformations in metastable austenitic steels. Acta Metall. Mater. 40 (7), 1703–1716.

Sugimoto, K.I., Kobayashi, M., Yasuki, S.I., 1997. Cyclic deformation behavior of a transformation-induced plasticity-aided dual-phase steel. Metall. Mater. Trans. A 28, 2637–2644.

Suiker, A.S.J., Turteltaub, S., 2005. Computational modelling of plasticity induced by martensitic phase transformations. Int. J. Numer. Meth. Eng. 63 (12), 1655–1693.

Thamburaja, P., Anand, L., 2001. Polycrystalline shape-memory materials: effect of crystallographic texture. J. Mech. Phys. Solids 49 (4), 709–737.

Turteltaub, S., Suiker, A.S.J., 2005. Transformation-induced plasticity in ferrous alloys. J. Mech. Phys. Solids. 53 (8), 1747–1788.

Wang, J.J., van der Zwaag, S., 2001. Stabilization mechanisms of retained austenite in transformation-induced plasticity steel. Metall. Mater. Trans. A 32 (6), 1527–1539.

Wechsler, M.S., Lieberman, D.S., Read, T.A., 1953. On the theory of the formation of martensite. Trans. Am. Inst. Miner. Met. Eng. 197 (11), 1503–1515.

Zanzotto, G., 1996. The Cauchy–Born hypothesis, nonlinear elasticity and mechanical twinning in crystals. Acta Cryst. A 52, 839–849.